Seventh Framework Programme

Theme 6 [SPACE]

Project: 607193 UERRA

Full project title:

Uncertainties in **E**nsembles of **R**egional **R**e-**A**nalyses

Deliverable D2.5

Report of results and datasets of two physics HARMONIE runs for spread estimation

WP no:	2
WP leader:	SMHI
Lead beneficiary for deliverable :	SMHI
Name of author/contributors:	Martin Ridal, Heiner Körnich, Esbjörn Olsson, Ulf Andrae
Nature:	Report
Dissemination level:	PU
Deliverable month:	12
Submission date:	February 16 , 2016

1. Introduction

Historical weather data is needed by numerous users, e.g. cities who want to determine climatological precipitation for a new parking area, insurance companies who want to estimate likelihood of extreme weather conditions, etc. Observations are often distributed too scarcely in space and time and capture only limited parameters such as temperature or relative humidity. In order to capture the entire state of the Earth system, the observations are combined with forecasts of numerical weather prediction models in a statistical process called data assimilation. The resulting state of the Earth system, which is as close to the true state of the atmosphere as can be simulated, is referred to as the analysis. National weather services produce 3-6-hourly analyses for initialization of their forecasting models. These analyses improve over the years due to updates in the numerical model, in the data assimilation methods and in the observing system. For climatological purposes, it is of importance to keep the producing system constant. This requirement leads to the need of so-called reanalysis (RA), where the latest model and methods are used to reprocess previous years.

Global reanalysis are produced by several institutes, such as the European Centre For Medium range Forecasts (ECMWF), National Centers for Environmental Prediction (NCEP), Japan Meteorological Agency (JMA) and others. However, these data sets do not provide the users with high-resolution regional reanalysis. There are clear needs for such datasets and in Europe there have been a series of efforts to create gridded datasets, however these efforts have been either limited to coarse resolution or fragmented into national datasets. Within the European Union funded project European Reanalysis and Observations for Monitoring (EURO4M), the work to answering these needs and produce RA products at an intermediately high-resolution (22 km but also with a downscaling to higher resolutions) started.

UERRA will address the limitations of what was possible to do in EURO4M but also focus on the uncertainties in the re-analyses. The time period will be much longer than in EURO4M to suite climate monitoring applications and the horizontal resolution will be higher. Advanced Ensemble Data Assimilation will also be used for a long time period to assess uncertainties in the RA themselves as well as high-resolution deterministic RA and other gridded datasets to be included in the evaluation of the uncertainties.

Within the framework of UERRA a regional re-analysis will be made using the HARMONIE (HIRLAM ALADIN Regional/Mesoscale Operational NWP In Europe) system. HARMONIE is a complete system for numerical weather prediction. It is developed in the HIRLAM (Hi-Resolution Limited Area Model)-consortium and builds upon the code of the models ALADIN (Aire Limitée Adaptation Dynamique Développement International), AROME (Applications of Research to Operations at MEsoscal) and ALARO (ALADIN and AROME combined model) developed in collaboration of Météo France and the consortia ALADIN and HIRLAM. The final HARMONIE-RA will be run from 1961-present.

To prepare the HARMONIE-RA and to examine the uncertainties in the reanalysis product, the possibilities to run HARMONIE with different schemes and models for physics and surface treatment is used. Specifically, two different physics schemes, ALADIN and ALARO, are used to produce a shorter RA of five years with a horizontal resolution of 11 km. Different ways of large scale mixing has also been tested in order to examine how the information from the global reanalysis can be optimally introduced into the regional reanalysis.

In this report, the modelling system with the different physics schemes, the data assimilation method, and the production scheme is explained in Section 2. Section 3 examines the different options for including the large-scale information from the global model. In Section 4, the results of the 5-year regional reanalysis, the verification against observations and the comparison with the global reanalysis ERA-Interim is presented. The report is concluded in Section 5.

2. Methods

The five year mini ensemble runs are performed using the HARMONIE system cycle 38h1.1. HARMONIE is basically a script framework that allows for different physics packages, surface schemes or data assimilation schemes. In the UERRA 5-year mini-ensemble runs the default setup is used with the exception that two different atmospheric physics schemes are used. One is the ALADIN synoptic scale scheme and the other the multi-scale ALARO scheme. Both are described in more detail below as well as the surface treatment which is common to both runs.

Both model versions are run with upper air data assimilation using a three dimensional variational assimilation (3D-Var) scheme and only conventional observations. This scheme as well as the employed surface assimilation is described in more detail below.

The experiments were run at the ECMWF facilities, each experiment in two streams (time periods) with one month overlap. Several changes in the script system were made to speed up the code compared to the reference version. The main achievement was to separate the analysis and forecast steps. In the UERRA runs the new analysis is started as soon as the first guess is available, i.e. the 6 hour forecast. The remaining forecast hours is run in parallel to the next analysis. This saves a lot of time in a reanalysis but is of no use for operational forecasts. The run time for the 5-year reanalysis is still rather long where one year takes slightly less than a month to complete. Five years will thus take about 3-4 months to run depending also on the machine load and access to the archiving system that sometimes can be slow.

Data assimilation

The observations are introduced into the model through data assimilation, both in the upper air and in the surface scheme.

Upper air

The assimilation scheme used in the 5-year runs is a 3D-Var assimilation scheme which creates an analysis by minimising a cost function (e.g. Gustafsson et al. 2001, Lindskog et al. 2001 or Brousseau et al. 2008):

$$J(x) = \frac{1}{2}(x - x_b)^T B^{-1}(x - x_b) + \frac{1}{2}(y - H(x))^T R^{-1}(y - H(x))$$

where x is the model state vector (containing the control variables vorticity, divergence, temperature, specific humidity and surface pressure), x_b is the first guess or background, in our case a 6-hour forecast.

y represents the observations while *H* is the observation operator, *B* is a matrix that describes the errors of x_b and *R* is a matrix that describes the errors of the observations *y*. It is assumed that the observation errors are spatially uncorrelated and thus, R is represented as a diagonal matrix. The background error matrix on the other hand, describes both spatial correlations and balances between variables. It uses a multivariate formulation based on the forecast errors of the control variables and horizontal spatial homogeneity and isotropy are assumed (Berre 2000). The background error correlations are calculated only once and do not take into account any time dependence (Brousseau et al. 2012) or any heterogeneous information in space (Montmerle and Berre 2010).

The observations included are the so-called conventional observation which include synoptic stations, ships, drifting buoys, aircraft observations and radio soundings. No remote sensing data is used for these experiments.

Surface

The surface observations are assimilated using an optimal interpolation (OI) method using CANARI (Code for the Analysis Necessary for ARPEGE for its Rejects and its Initialization) and SURFEX (surface externalisée).

CANARI (Taillefer, 2002) is a part of the IFS/ARPEGE (Integrated Forecast System/Action de Recherche Petite Echelle Grande Echelle) (Bubnová et al. 1995; ALADIN International Team 1997) source code and were developed to provide both surface and upper air ARPEGE/ALADIN analysis based on the optimum interpolation (OI) method. Together with SURFEX however, it is only used for the horizontal interpolation (Seity et al 2011).

With SURFEX the surface analysis is performed in two steps. First CANARI finds the analysis increments in each grid point based on observations minus first guess. In the next step a consistent update of the SURFEX surface fields is made based on analysis increments interpolated to all grid points by CANARI.

SURFEX has 4 tiles; nature, sea, inland waters (lakes and rivers) and town. The Interactions between Soil, Biosphere, and Atmosphere (ISBA) parameterization (Noilhan and Planton, 1989) is by default used at nature points updating temperature, water and ice in 3 layers (surface, soil and deep soil) and the properties of a single layer of snow. Only surface temperature is updated at sea and lake surfaces.

In the UERRA-RA, only synoptic observations are used to analyse 2 meter temperature (T2m), 2 meter relative humidity (RH2m) and Snow Water Equivalent (SWE).

The ALADIN and ALARO setups

The basis for the ALADIN and ALARO setups is the limited area model (LAM) version of the ARPEGE-IFS (Bubnová et al. 1995; ALADIN International Team 1997). It comprises a non-hydrostatic spectral dynamical core with semi-implicit time stepping and semi-Lagrangian advection. In the horizontal resolution used in UERRA, 11km, the model is applied using the hydrostatic assumption.

The ALARO physics package is specifically designed to be run at horizontal resolutions of around 5-km grid spacing toward convection-permitting scales. To handle convection properly on these scales, the prognostic convection scheme called Modular Multiscale Microphysics and Transport (3MT) was developed by Gerard et al. (2009) for ALARO. Radiation is parameterized following Ritter and Geleyn (1992) with some modifications. A prognostic microphysics scheme is used in combination with a

statistical scheme for the sedimentation of precipitating particles (Geleyn et al. 2008). Turbulence in ALARO is parameterized with a pseudo-prognostic turbulent kinetic energy (TKE) scheme as described in Váňa et al. (2008).

In ALADIN the radiative transfer in the atmosphere (gaseous, clouds, ozone, and aerosols) with the surface is described using the RRTM scheme (Rapid Radiative Transfer Model) for longwave radiation (Mlawer et al., 1997) and the six-band Fouquart–Morcrette scheme for shortwave radiation (Fouquart and Bonnel, 1980; Morcrette, 1991). Several phenomena linked to the subgrid orography, such as gravity waves, their reflection and trapping, as well as upstream blocking, are taken into account (Catry et al., 2008). The transport in the atmospheric boundary layer is represented with a diffusion scheme based on prognostic turbulent kinetic energy (Cuxart et al., 2000) using the Bougeault and Lacarrère (1989) mixing length, and on a mass-flux shallow convection scheme using a CAPE closure (Bechtold et al., 2001). Deep convection is represented with a mass-flux scheme based on a moisture convergence closure (Bougeault, 1985). A statistical cloud scheme (Smith, 1990; Bouteloup et al., 2005) is used for the representation of stratiform clouds. Microphysical processes linked to resolved precipitations such as auto-conversion, collection, evaporation, sublimation, melting and sedimentation are explicitly represented (Lopez, 2002).

Both ALADIN and ALARO are coupled to the externalized version of the Méso-NH surface scheme, called Externalized Surface (SURFEX). Here each grid box is split into four tiles: land, towns, sea, and inland waters (lakes and rivers). The Interactions between Soil, Biosphere, and Atmosphere (ISBA) parameterization (Noilhan and Planton 1989) with two vertical layers inside the ground is activated over land tile. The Town Energy Budget (TEB) scheme used for urban tiles (Masson 2000) simulates urban microclimate features, such as urban heat islands. Sea tiles use the Exchange Coefficients from Unified Multicampaigns Estimates (ECUME) parameterization (Belamari and Pirani 2007). It is a bulk iterative parameterization developed in order to obtain an optimized parameterization covering a wide range of atmospheric and oceanic conditions. Based on the Liu–Katsaros–Businger algorithm (Liu et al. 1979), ECUME includes an estimation of neutral transfer coefficients at 10 m from a multicampaign calibration derived from 5 flux measurement campaigns. Concerning inland waters, the classic Charnock's (Charnock 1955) formulation is used. Output fluxes are weight averaged inside each grid box according to the fraction occupied by each respective tile, before being provided to the atmospheric model. Physiographic data are initialized due to the ECOCLIMAP database (Masson et al. 2003) at 1-km resolution.

3. Mixing of large scales

NWP on a regional domain requires a coupling system that provides lateral boundary information during the time integration step. The coupling system is often a global NWP model run on a coarser grid mesh than the regional model. Global models are generally better at representing large scale features, e.g. Rossby waves with a length scale of 10^3 km, which is essential to get the position of the synoptic high- and low pressure systems right. Blending, or large scale mixing, refers to the methodology of introducing the large scale features of the host model into the initial condition of a regional model.

There are different ways to do this and in the HARMONIE framework two methods are implemented. The first method, LSMIXBC, combines the large scale spectral components from the first boundary file with the small scale components from ALADIN/ALARO into a modified field used as first guess in the 3DVAR analysis. The second method adds a penalty term, Jk, to the cost function in 3D-Var that

measures the distance between the model state and the large scales from the host model (Guidard and Fischer, 2008). It has been shown by Dahlgren (2012) that the latter method gives somewhat better results. Thus, in this study the Jk-formulation will be the choice.

In the 5-year mini-ensemble run, large scales from ERA interim are mixed in via a Jk-term in the 3D-Var minimisation. This means that the large scale mix will be added as an extra constraint in the 3D-Var.

From ERA interim the analyses are used. This implies that there is a risk of using the same observations twice, however, the verification of the experiments run with analyses instead of forecasts verified much better. An example from January 2006 with ALADIN is shown in Figure 1. The green line represents the experiment using ERA-interim forecasts (jk1) while the red line is the same experiment but using ERA-interim analyses for the Jk-term. The upper lines show the model error (standard deviation) and the lower ones show the bias of wind speed at 300 hPa.

After the five years were completed however, it has been discovered that there is an error in the implementation of Jk. What effect this will have on the resulting fields needs to be investigated.

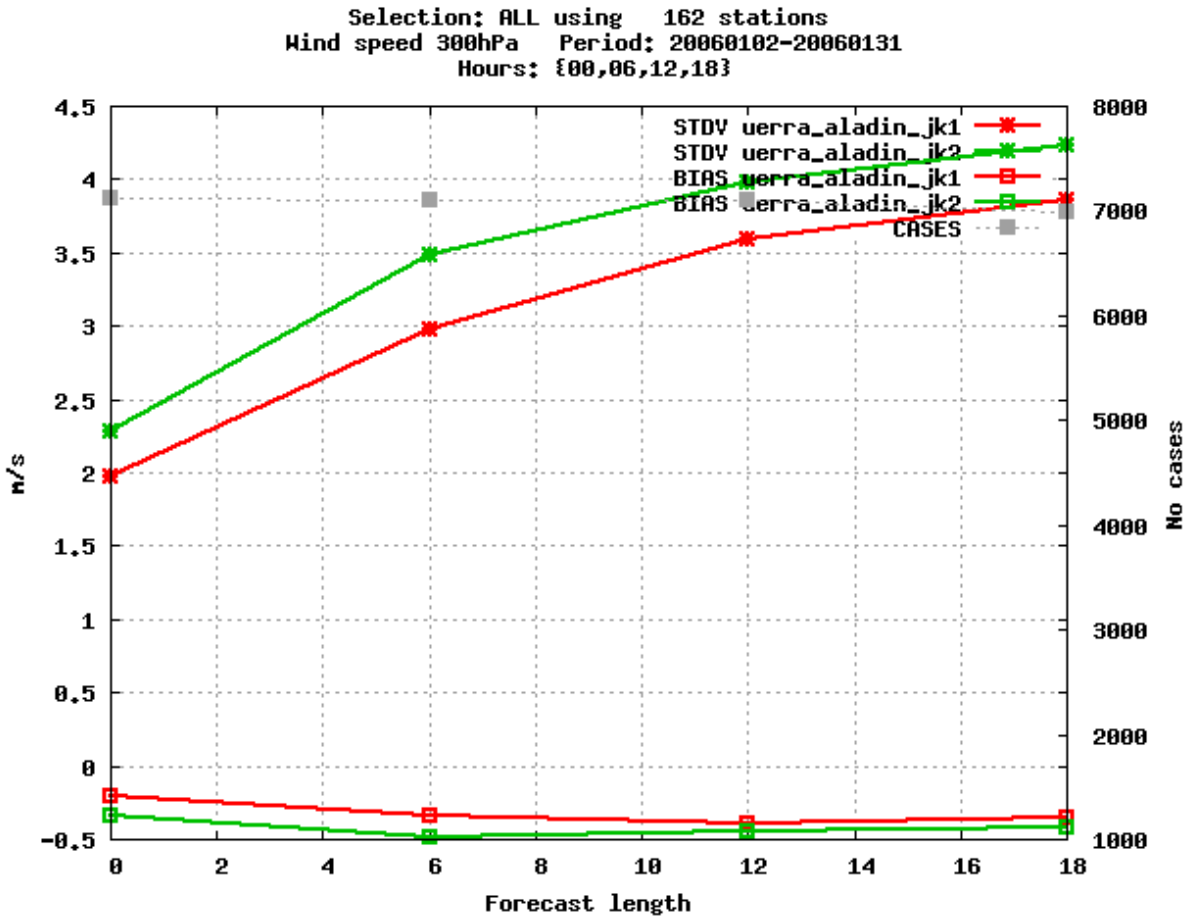

Figure 1. Comparison between two ALADIN experiments using Jk with ERA-interim forecasts (green) and ERA-interim analyses (red)

4. Results

The two reanalysis experiments were run from January 2006 to December 2010. Both models include data assimilation using only conventional observations, i.e. SYNOP observations, ships, drifting buoys, aircraft observations and temperature soundings. For the surface assimilation temperature and relative humidity at two meters as well as snow water equivalent, all from SYNOP stations are included. In the observation monitoring shown here only the upper air observations are shown.

The results presented here do not include the town energy balance (TEB) for ALARO due to a mistake in the model setup. This affects the results for the ALARO runs over towns but, as a sensitivity experiment showed, over the total area the effect is not visible. Thus, the results presented here are not affected by the lack of TEB in the ALARO-RA. It was also discovered that a few surface fields were not archived in the ALADIN runs. These fields may be of interest when using the output data from the 5-year runs. Therefore, these fields are reproduced for the five years 2006-2010. This rerun is made as part of the long UERRA reanalysis.

The error in the large scale mixing term (see Section 3) can also affect the results. It is believed however, that the main results and conclusion will not be affected since in the areas of good observation coverage the Jo-term dominates the cost function described above. It is only in areas with very few observations that the Jk-term will be dominating. The verifications are made against observations and thus it is assumed that the effect of an error in Jk will not change the conclusions from the general verification scores.

Observation monitoring

Observation monitoring is a useful tool to check that the data assimilation is working as expected. In an operational environment it is also used to monitor the incoming observations in order to discover if any observation type is partly or totally missing.

When it comes to observation usage, the difference between ALADIN and ALARO is very small. The number of observations that enter the model, i.e. before the screening, should be exactly the same. The number of observations that are actually used in the minimisation can on the other hand differ slightly. The reason is that the two models evolve differently and observations can be screened due in the first guess check (too large departure from the first guess) or in the variational quality control. In the log files from the experiments it is noted that the difference between ALADIN and ALARO is never more than 5 observations per observation type. Therefore only examples of the observation monitoring for ALARO is shown below.

It could be expected that the number of observations should increase when comparing 2006 with 2010. However, 5 years is a fairly short time period. Still the number of observations increase over the period but not that much. The largest increase can be found in the aircraft observations, especially at high altitude, i.e. cruising level. Examples of the number of aircraft observations for January 2006 and 2010 that enters the ALARO minimisation are shown in Figure 2 and Figure 3 respectively. The different panels show the number of observations at different pressure levels. The largest number of observations as well as the largest difference between 2006 and 2010 is seen at 275 hPa. Note that the scales on the y-axis are different. Examples of the number of geopotential height observations from SNYOP stations that are used in the minimisation are shown in Figure 4 and Figure 5. The first are for January 2006 while the

latter shows January 2010. Note that there is an increase in the number of observations from ~1700 as maximum in 2006 to almost 1850 in 2010.

Shown here are the numbers of observations that enter the minimisation. The minimisation is run after the screening in which some observations can be sorted out for reasons like redundancy, too large departure from the first guess and similar. In the 5-year runs, however, the number of observations that enters the screening is very similar to the number of observations that leaves the screening and enters the minimisation. This implies that the quality of the observations is good and there is no need for data reduction. If satellite data, for example, should be used, the difference would be rather large before and after the screening. The reason is that most satellite observations are made with a very high resolution and a data reduction is needed in order to avoid correlated errors and to speed up the data handling.

Another example of the importance of observation monitoring is to check if the assimilation is working properly. This can be done by comparing the first guess (background) and analysis departure, i.e. how much the observations differ from the first guess and from the resulting analysis. If everything is working well the analysis departure should be smaller than the first guess departure. This means that the model has adjusted to the observations. How big this adjustment is will depend on both the background and the observation error.

Examples of the first guess departures compared to the analysis departures are shown in Figure 6 and Figure 7, again for ALARO only, since the two model versions are very similar in behaviour, and for January 2006 and 2010 respectively. It is seen that the root mean square error (RMS) decrease for the observation minus analysis (red lines with dots) compared to the observation minus first guess (blue line with dots). The systematic errors also decrease for the analysis (red) compared to the first guess (blue). It can also be noted that the observation minus analysis difference as well as the observation minus first guess difference is smaller for 2010 than for 2006. This can indicate the quality of the observations and/or the quality of the short forecast used as first guess has increased. It can, however, also just be weather dependent.

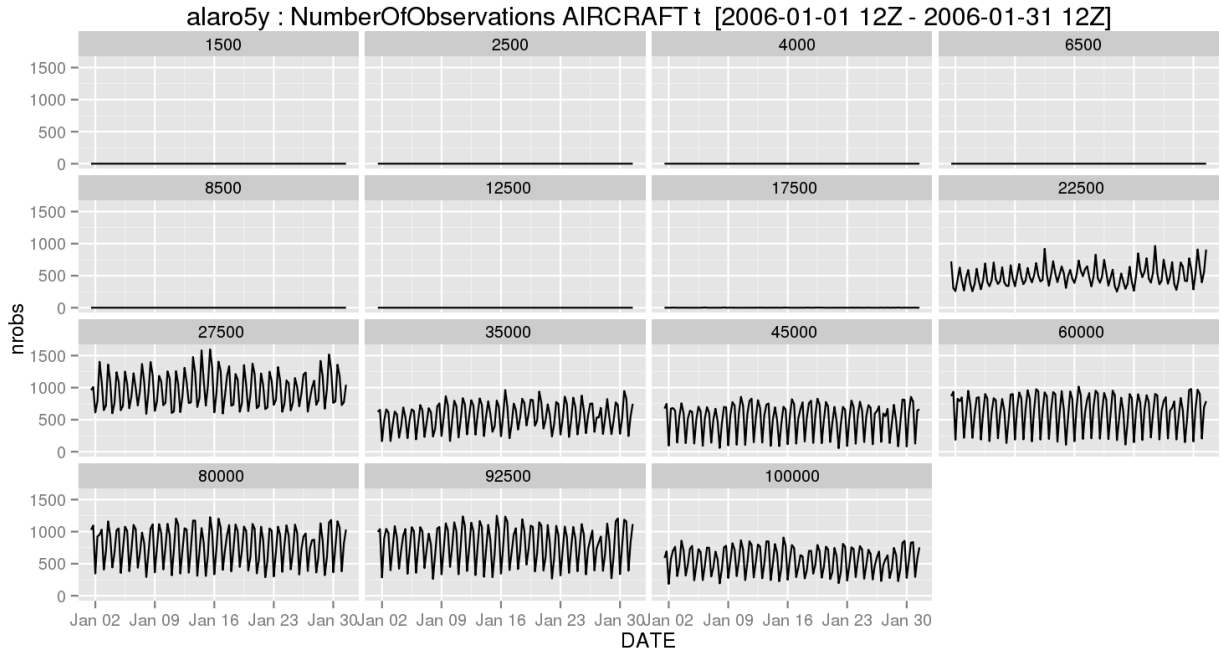

Figure 2. The number of temperature observations used in the ALARO minimization in January 2006. The different panels represent different pressure levels where the pressure is given in Pa.

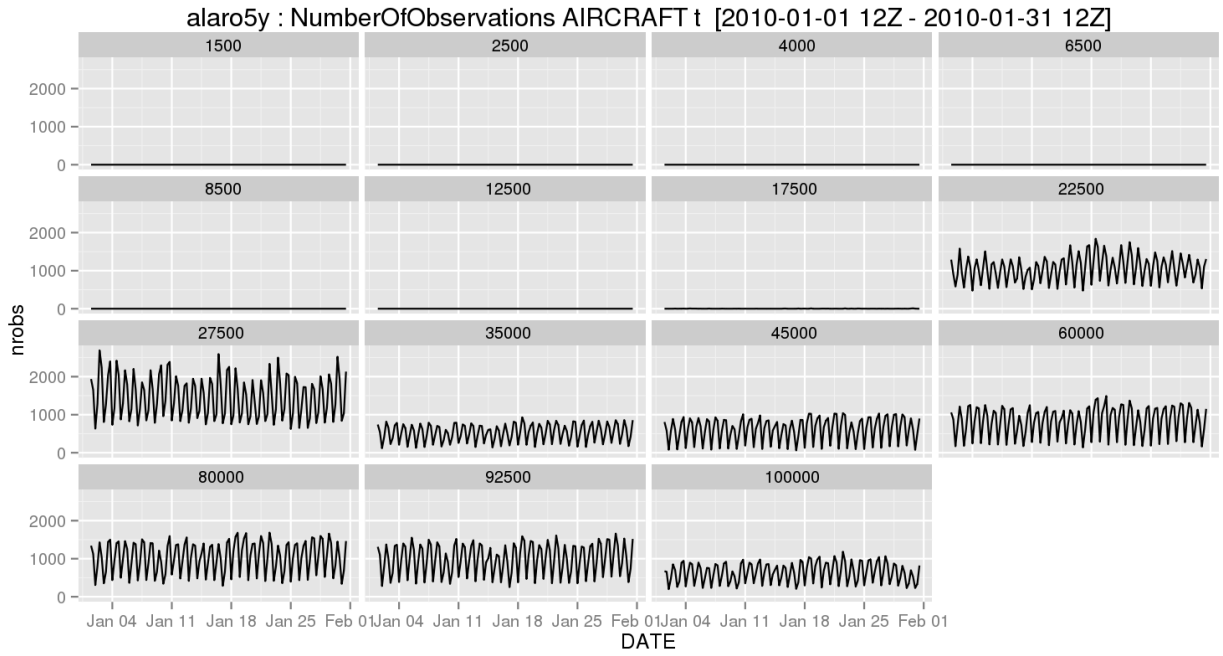

Figure 3. The number of temperature observations used in the ALARO minimization in January 2010. The different panels represent different pressure levels where the pressure is given in Pa.

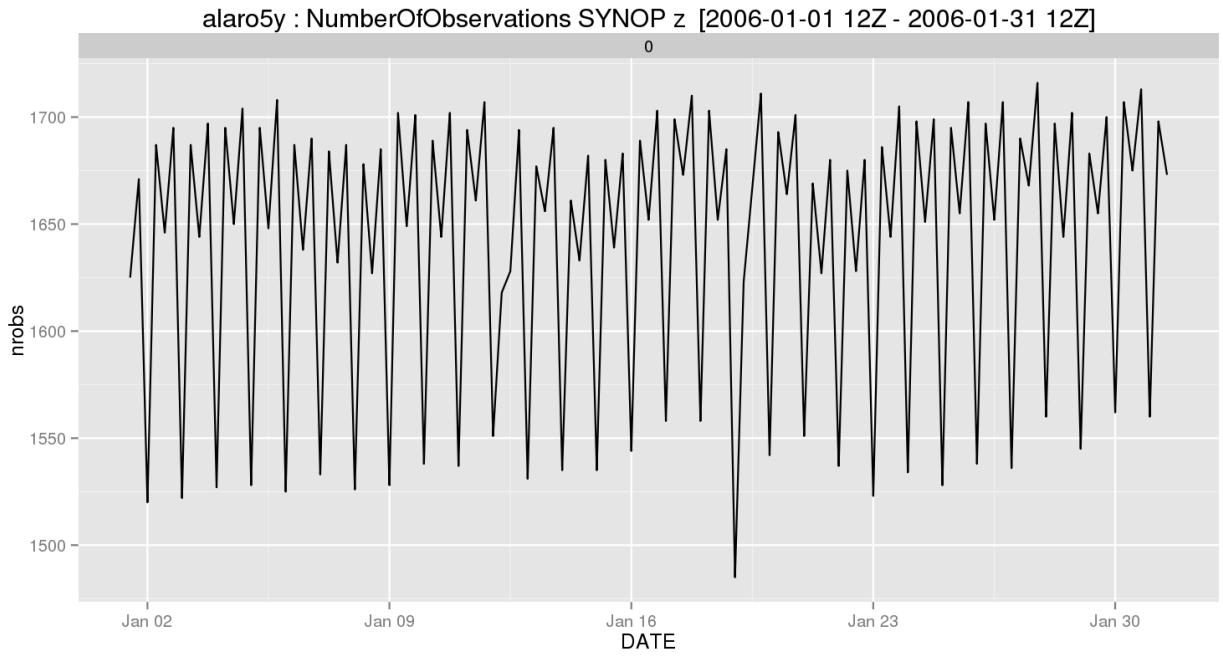

Figure 4. The number of geopotential height observations from SYNOP stations used in the ALARO minimization in January 2006.

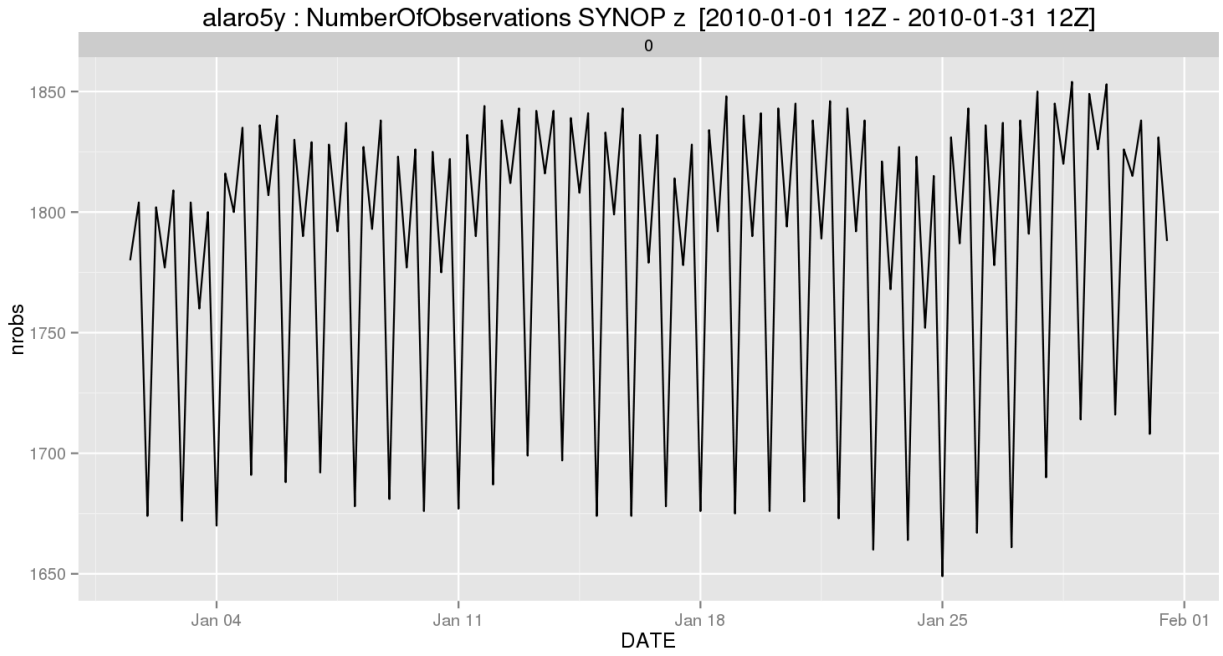

Figure 5. The number of geopotential height observations from SYNOP stations used in the ALARO minimization in January 2010.

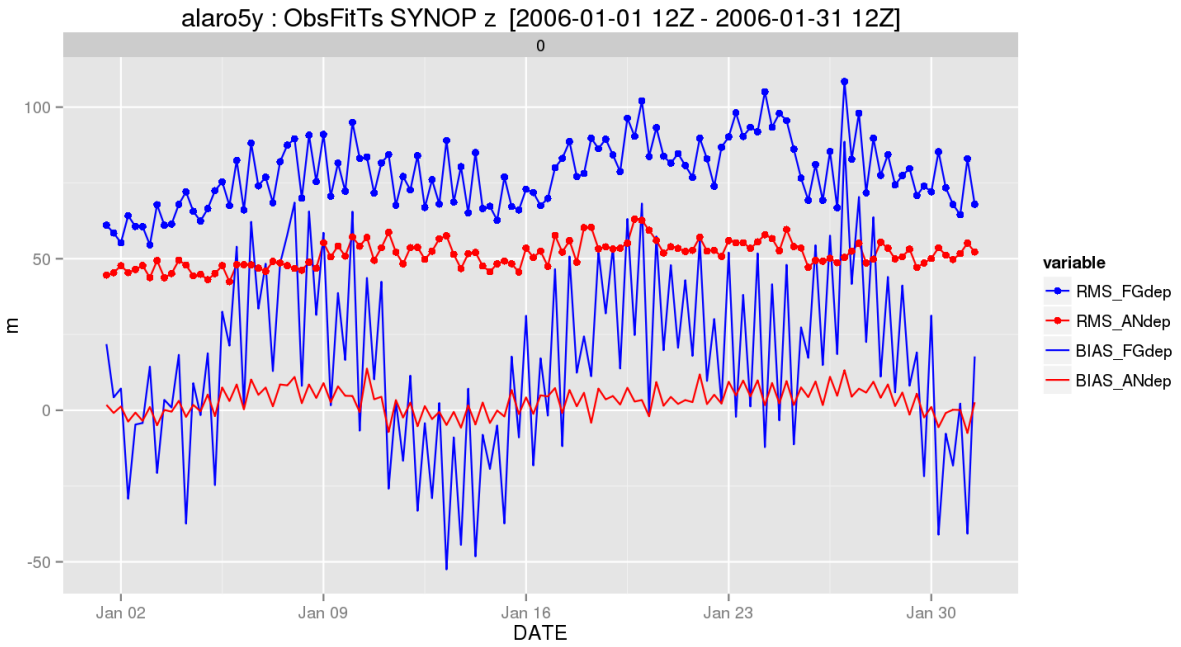

Figure 6. Observation - first guess departure (blue) and observation - analysis departure (red) of geopotential height from SYNOP observations for January 2006. Lines with dots are root mean square error (RMS) and lines without dots are the systematic errors (bias)

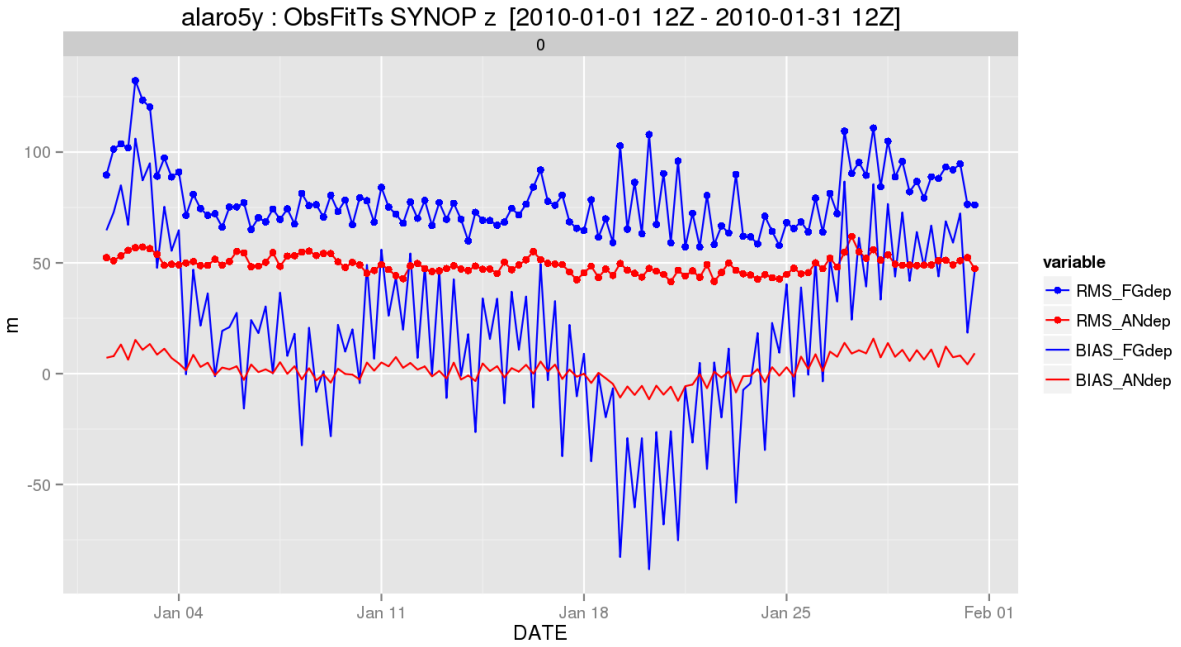

Figure 7. Observation - first guess departure (blue) and observation - analysis departure (red) of geopotential height from SYNOP observations for January 2010. Lines with dots are root mean square error (RMS) and lines without dots are the systematic errors (bias)

Climatology of the 5-year reanalyses

In order to examine the two 5-year reanalyses (RA) produced with the model physics of ALADIN and ALARO, statistics over the years 2006 to 2010 are calculated. These statistics will be compared to equivalent figures from ERA-Interim reanalysis, where the coarser ERA-Interim grid is projected onto the same grid as the UERRA-RA. The statistics are calculated separately depending on month and hour-of-day, focusing on 0 UTC in January, and 12 UTC in July.

The first two rows of Figure 8 show the monthly mean and daily standard deviation of temperature at 0 UTC in January for ERA-interim, ALADIN-RA and ALARO-RA. The monthly mean temperature (first row in Figure 8) looks very similar in all three data sets. It should be noted that the higher resolution of the UERRA reanalysis can be clearly seen in connection to the higher resolved topography compared to ERA-Interim. The daily standard deviation for temperature (second row in Figure 8) is similar in all three data sets. Differences can be seen, for example, in northern Africa with more variance in ALARO-RA and in eastern and northern Europe with less variance in ALARO-RA compared to the other two reanalyses.

The last two rows of Figure 8 display the monthly mean and daily standard deviation of temperature at 12 UTC in July for all three re-analyses. For the monthly mean fields (third row in Figure 8), the UERRA re-analyses provide clearly more spatial detail as mentioned above. For the standard deviation (fourth row in Figure 8), ERA-Interim and ALADIN-RA show similar behavior except for the finer details produced in ALADIN-RA. On the other hand, the ALARO-RA shows stronger temperature variance in middle Europe and northern Africa. The increased variance in these areas can be a result of the error found in the Jk-term in the minimization. It needs however a deeper going analysis.

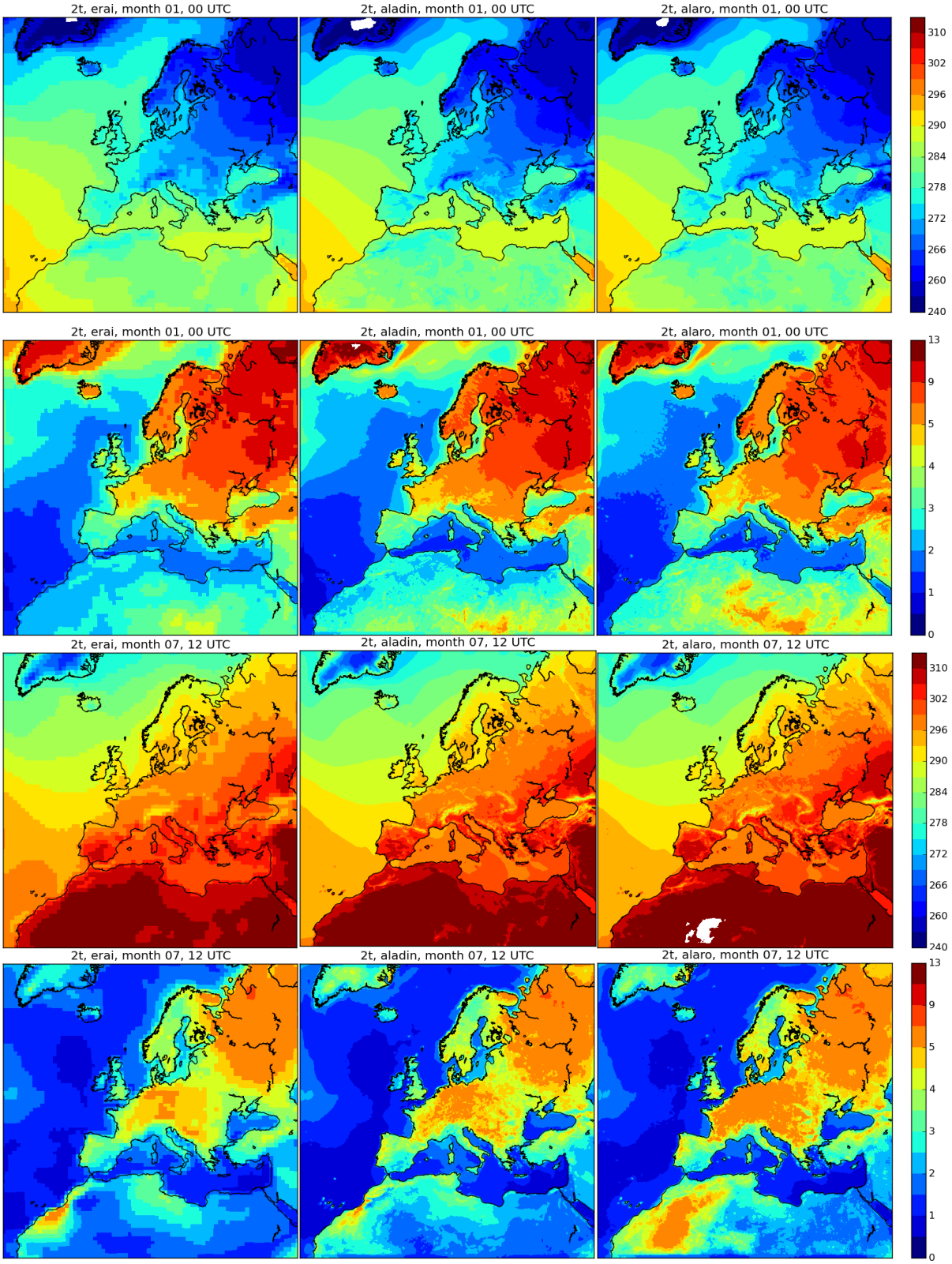
2t, erai, month 01, 00 UTC
2t, aladin, month 01, 00 UTC
2t, alaro, month 01, 00 UTC
310
302
296
290
284
278
272
266
260
240
2t, erai, month 01, 00 UTC
2t, aladin, month 01, 00 UTC
2t, alaro, month 01, 00 UTC
13
9
5
4
3
2
1
0
2t, erai, month 07, 12 UTC
2t, aladin, month 07, 12 UTC
2t, alaro, month 07, 12 UTC
310
302
296
290
284
278
272
266
260
240
2t, erai, month 07, 12 UTC
2t, aladin, month 07, 12 UTC
2t, alaro, month 07, 12 UTC
13
9
5
4
3
2
1
0

Figure 8. Monthly mean (first and third row) and daily standard deviation (second and fourth row) of temperature in K for January at 0 UTC (first two rows) and July at 12 UTC (last two rows), averaged over years 2006 to 2010, for ERA-interim (left), UERRA-ALADIN (middle), UERRA-ALARO (right). The colour intervals for the standard deviation are in 0.5 K steps up to 5 K, then in 2 K steps up to 13 K. White areas mark values beyond the given limits.

Figure 9 shows the mean and daily standard deviation of the wind strength at 10 metres above ground for January at 0 UTC (first two rows) and for July at 12 UTC (last two rows). Generally, all re-analyses display similar means and standard deviation, while the UERRA re-analyses are able to represent finer spatial scales visible in features connected to topography.

In January, strong near-surface winds prevail over the North Atlantic continuing across middle-northern Europe (first row of Figure 9). The dataset ALADIN-RA (middle column) differs notably from the other two with generally weaker winds, especially over Northern Africa. This difference between the ALADIN-RA and ALARO-RA (middle and right column) is strongest at 0 UTC and minimizes at 12 UTC (not shown). This can be due to the daily cycle of the 10m-wind and further studies are needed in order to understand the model differences that give rise to this behavior.

The strongest variability in January is also seen over the North Atlantic and the related corridor over continental Europe (second row in Figure 9). The three reanalysis provide comparable magnitude. However, the higher resolution for the UERRA-reanalysis leads to stronger wind variance in mountain ranges, such as the Alps, the Atlas Mountains and the Caucasus Mountains. The daily cycle in the daily standard deviation of the 10m-wind strength is weak in the re-analyses, except for Northern Africa where all three re-analyses show largest variance at 12 UTC (not shown).

In July, the near-surface winds over the Northern Atlantic are weaker on average (third row in Figure 9). Over the continent, the UERRA re-analyses by ALADIN and ALARO (middle and right) show generally weaker 10m-winds than ERA-Interim (left). Resembling the results for January, ALADIN shows slightly weaker winds at 12 UTC in Northern Africa. Concerning the daily cycle, the same difference between ALADIN and ALARO is noted in Northern Africa, where ALADIN shows considerably weaker winds at 00 UTC than the other reanalysis (not shown). The ALARO-RA displays on average weaker 10m-winds in the Northern continental part of the domain.

The 10m-wind variability in July at 12 UTC can be seen in the last row of Figure 9. Both ALADIN- and ALARO-RA (middle and right) have in general weaker wind variability than ERA-Interim (left). The strongest difference is visible for ALARO-RA (right) over Northern continental part. This difference prevails even throughout the daily cycle (not shown). A further analysis of this issue is recommended.

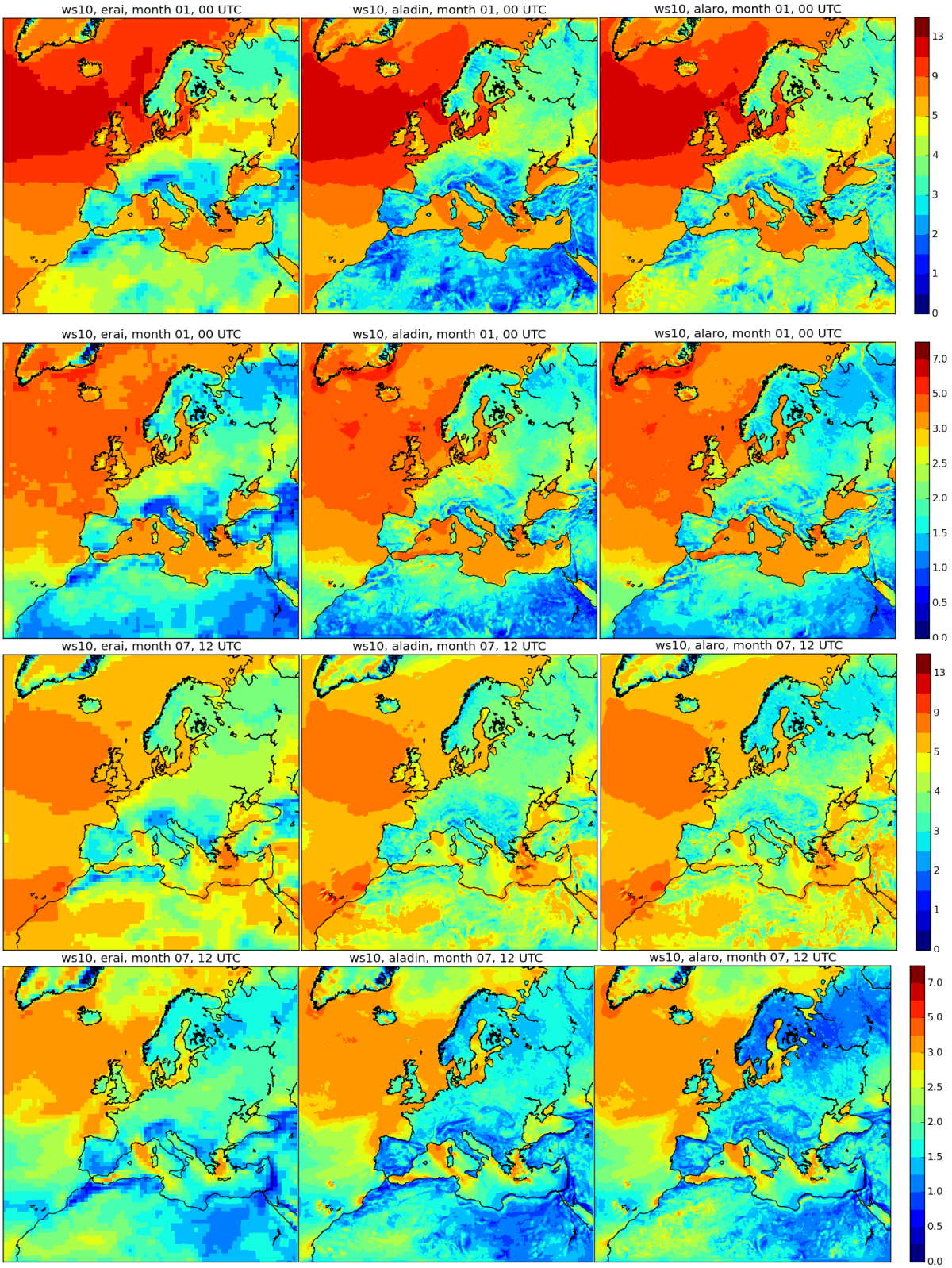
ws10, erai, month 01, 00 UTC
ws10, aladin, month 01, 00 UTC
ws10, alaro, month 01, 00 UTC
13
9
5
4
3
2
1
0
ws10, erai, month 01, 00 UTC
ws10, aladin, month 01, 00 UTC
ws10, alaro, month 01, 00 UTC
7.0
5.0
3.0
2.5
2.0
1.5
1.0
0.5
0.0
ws10, erai, month 07, 12 UTC
ws10, aladin, month 07, 12 UTC
ws10, alaro, month 07, 12 UTC
13
9
5
4
3
2
1
0
ws10, erai, month 07, 12 UTC
ws10, aladin, month 07, 12 UTC
ws10, alaro, month 07, 12 UTC
7.0
5.0
3.0
2.5
2.0
1.5
1.0
0.5
0.0

Figure 9. Monthly mean (first and third row) and daily standard deviation (second and fourth row) of wind strength in 10 metre height above ground in m/s for January at 0 UTC (first two rows) and July at 12 UTC (last two rows), averaged over years 2006 to 2010, for ERA-interim (left), UERRA-ALADIN (middle), UERRA-ALARO (right). The colour intervals for the mean are in steps of 0.5 m/s from 0 to 5 m/s, then in steps of 2 m/s from 5 to 15 m/s. The colour intervals for the standard deviation are in steps of 0.25 m/s, from 0 to 3 m/s, then in steps of 1 m/s from 3 to 8 m/s. White areas mark values beyond the given limits.

Figure 10 shows the monthly mean and standard deviation of the total precipitation for January initialized at 12 UTC and for July at 00 UTC. The total precipitation is given as the difference between the accumulated 24-hour and 12-hour forecasts. Thus it is valid from 0 to 12 UTC for January and from 12 to 0 UTC for July. Units are given in mm per 12 hours. In general, the higher resolution of the UERRA-re-analyses creates finer details than in ERA-interim, visible at coast lines and mountain ranges. The sharper gradients in topography lead locally to larger amplitudes both in the mean and in the standard deviation for the UERRA re-analyses compared to ERA-Interim. The local character of precipitation, especially in summer time, leads to more noise in the patterns than for temperature and wind.

In January, the largest mean precipitation (first row in Figure 10) occurs over the North Atlantic and on some western coasts, such as the Norwegian, northern Iberian or Balkan coasts. Except for the above mentioned finer details in the UERRA re-analyses compared to ERA-Interim, all three datasets have similar distribution and amounts in the mean.

The daily standard deviation of the total precipitation in January (second row in Figure 10) is largest over the North Atlantic and around the Mediterranean. Especially for the latter, ALADIN-RA (middle) shows clearly larger variance than the other two datasets. In July, the largest mean precipitation during 12 and 0 UTC (third row in Figure 10) occurs over land for Middle- and Northern Europe. Both UERRA-reanalysis show generally higher values than ERA-Interim. The largest mean are shown in ALADIN-RA, clearly visible in Middle- and Northern Europe. Over Central and Western Europe, the daily cycle is similar in all re-analyses with higher precipitation in the second half of the day (12-0 UTC) than in the first half of the day (0-12 UTC)(not shown). However, the diurnal cycle differs in the northeastern part of the domain, where ERA-Interim and ALADIN-RA have stronger precipitation in the first half of the day, while ALARO-RA shows stronger precipitation in the second half (not shown). This behavior needs to be examined in more detail.

The daily standard deviation of the total precipitation in July (fourth row in Figure 10) has largest amplitude over land north of the Mediterranean. Both UERRA re-analyses display stronger variance than ERA-Interim. An interesting feature is the band of precipitation along the Atlas Mountains with clearly stronger mean precipitation and variability in the UERRA re-analyses than in ERA-Interim.

In order to examine the daily cycle, only the accumulations from 0 to 12 UTC and from 12 to 0 UTC are compared. For January, none of the three re-analyses display a clear daily cycle for the monthly mean or the daily standard deviation of the total precipitation (not shown). The diurnal cycle in the precipitation variability for July is also difficult to judge from the noisiness of the figures (not shown). A clear cycle however, is seen for the precipitation band along the Atlas Mountains with larger amplitudes in the second half of the day than in the first (not shown).

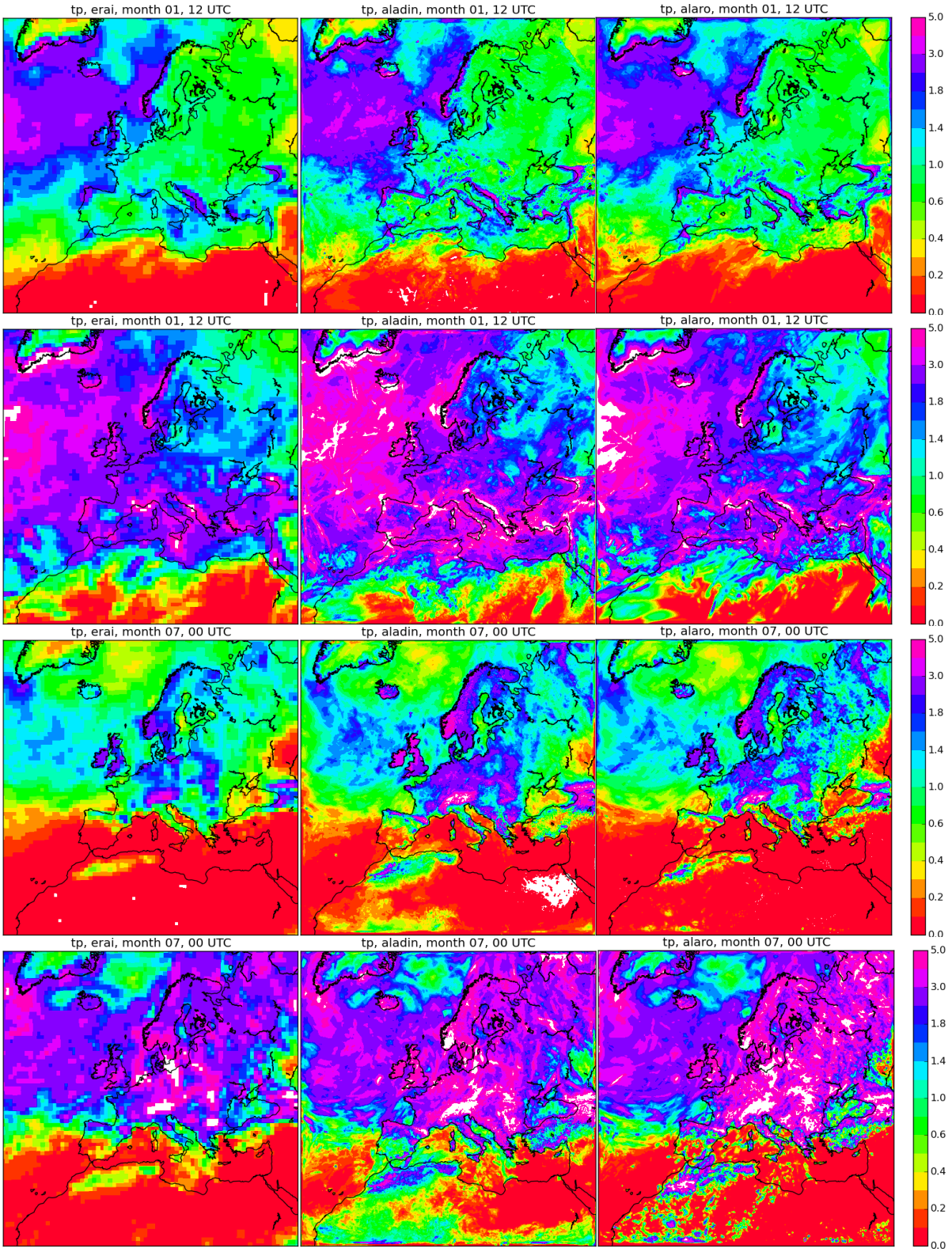

Figure 10. Monthly mean (first and third row) and daily standard deviation (second and fourth row) of total precipitation in mm/12hours for January initialized at 12 UTC (first two rows) and July at 00 UTC (last two rows), averaged over years 2006 to

2010, for ERA-interim (left), UERRA-ALADIN (middle), UERRA-ALARO (right). The difference between the accumulated forecasts for 24 hours and 12 hours is shown. The colour intervals for the mean and standard deviation are in steps of 0.1 mm/12hours from 0 to 0.5 mm/12hours, in steps of 0.2 mm/12hours from 0.6 to 2 mm/12hours, then in steps of 1 mm/12hours from 2 to 5 mm/12hours. White areas mark values beyond the given limits.

Mean error and spread of HARMONIE-RA mini-ensemble

In this section, the statistics for the difference between ALADIN- and ALARO-RA, averaged over the years 2006 to 2010 are presented, focusing on the months of January and July. The examined variables are the 2m-temperature, 10m-wind strength, and 12-hour accumulated total precipitation. The mean difference will provide an estimate for the systematic error or accuracy in the reanalysis, while the standard deviation of the reanalysis difference yields a measure for the unbiased uncertainty or precision of the reanalysis.

The mean 2m-temperature difference in January at 0 UTC (**Fel! Hittar inte referenskälla.**) shows generally a good agreement between ALADIN- and ALARO-RA with difference smaller than 1 K. However, ALADIN is clearly colder than ALARO in the northern-eastern part of the domain, but ALADIN is warmer than ALARO in the larger part of Northern Africa, Turkey and Caucasus. These differences can amount locally up to 3 K, rarely 5 K. During different hours of the day the pattern remains very similar, but with smallest amplitude at 12 UTC (not shown).

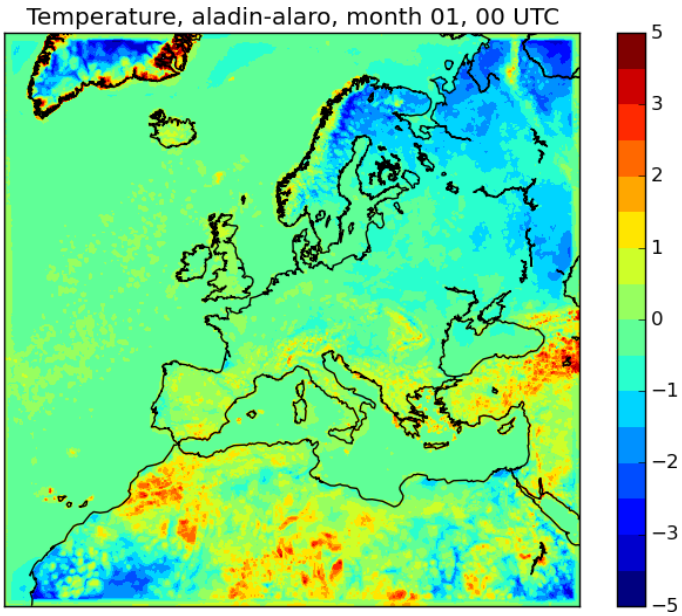

Figure 11. Mean temperature difference between ALADIN-RA and ALARO-RA for January at 0 UTC. The colour intervals are in steps of 0.5 between -3 and +3 K, and in steps of 1 K between absolute values of 3 and 5.

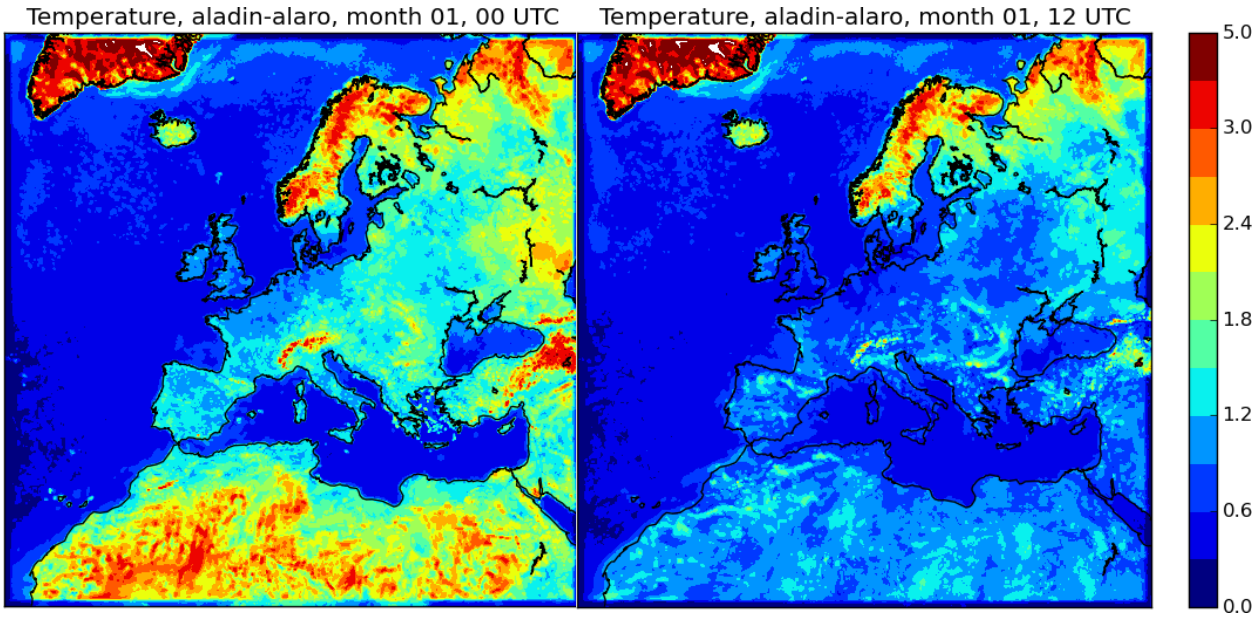

Figure 12. Daily standard deviation of temperature difference between ALADIN-RA and ALARO-RA in January. Panel depict the values for 0 (left) and 12 UTC (right). The colour intervals are in steps of 0.3 up to 3 K, and in steps of 1 K up to 5. White areas mark values beyond the given limits.

Figure displays the standard deviation of the temperature difference between ALADIN- and ALARO-RA for January. Each panel shows the values for different hours of the day. In general, the standard deviation is larger over Northern land cover. Largest values of up to 5 K are reached over Greenland. For the southern part of the domain, especially over Northern Africa, the precision of the reanalysis varies throughout the day with larger uncertainty at 0 and 6 UTC than at 12 and 18 UTC. The Caucasus region shows large uncertainty at all hours except around 12 UTC.

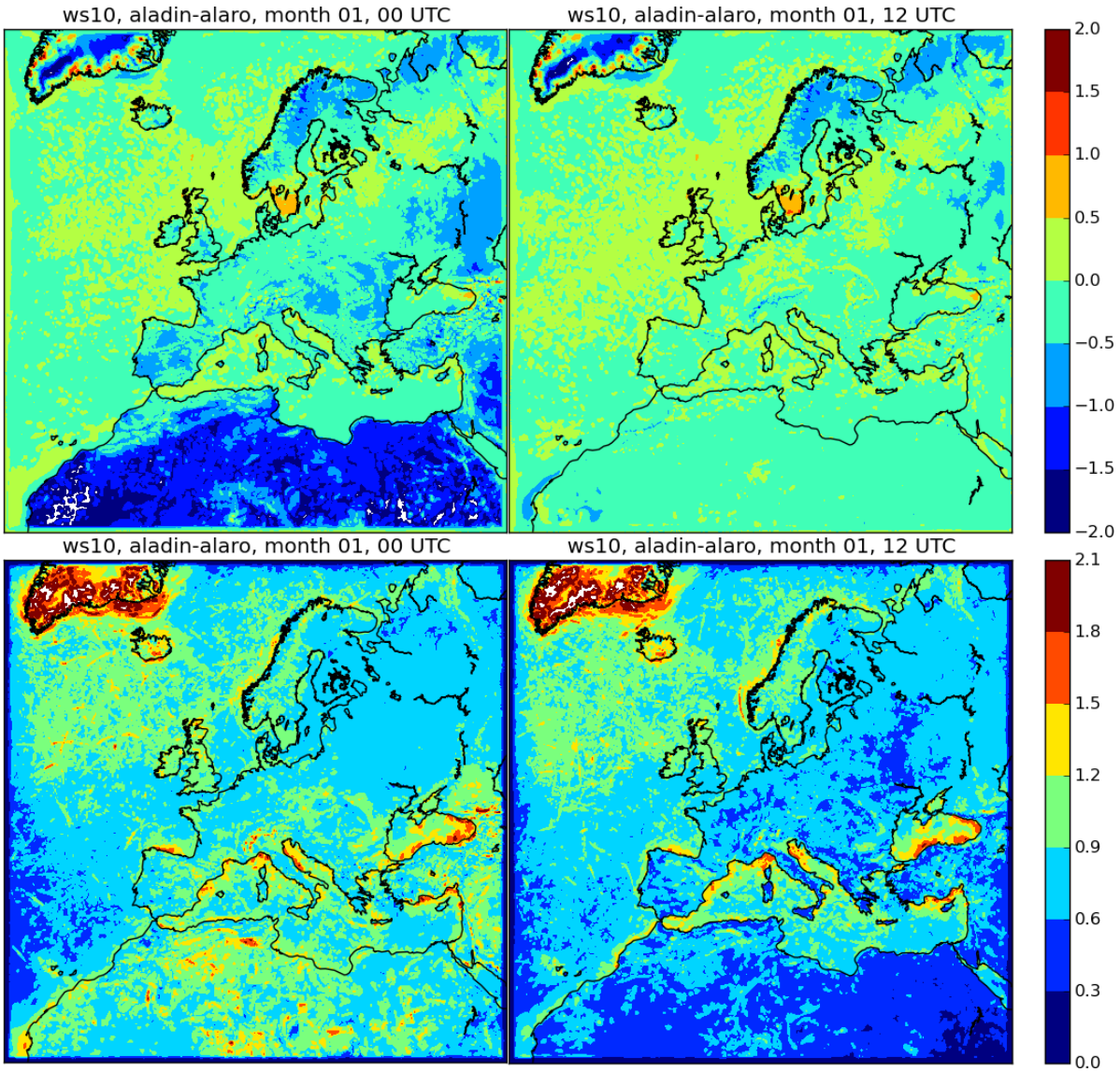

Figure 13. Mean (upper row) and daily standard deviation (lower row) of 10m-wind speed difference between ALADIN- and ALARO-RA in January. Left and right panels depict the values for 0 and 12 UTC, respectively. The colour intervals are in steps of 0.5 m/s for the mean and in steps of 0.3 m/s for the standard deviation.

The statistics for the 10m-wind speed difference between ALADIN- and ALARO-RA is displayed in Figure . Over large parts of Europe, the mean winds agree within 1 m/s difference with a standard deviation under 1.2 m/s.

Larger mean differences in the 10m-wind speed appear in Northern Africa at 0 UTC (upper left in Figure), and also at 6 and 18 UTC (not shown), with values up to 2 m/s. Simultaneously, larger standard deviation can be found in both 10m-wind and 2m-temperature differences in Northern Africa. At 12 UTC, the mean difference in 10m-wind speed in Northern Africa vanishes, and also the standard deviations in 2m-temperature and 10m-wind are much reduced.

It is interesting to note that enlarged standard deviation of the 10m-wind speed difference can be found along certain coast lines during all hours of the day (see lower row of Figure for 0 and 12 UTC). It would be of interest to examine closer this phenomenon.

The largest standard deviation for the 10m-wind speed differences are seen over Greenland with values slightly larger than 2 m/s. The large uncertainty, closeness to the border and high topography point to caution in usage of the UERRA-reanalysis for Greenland.

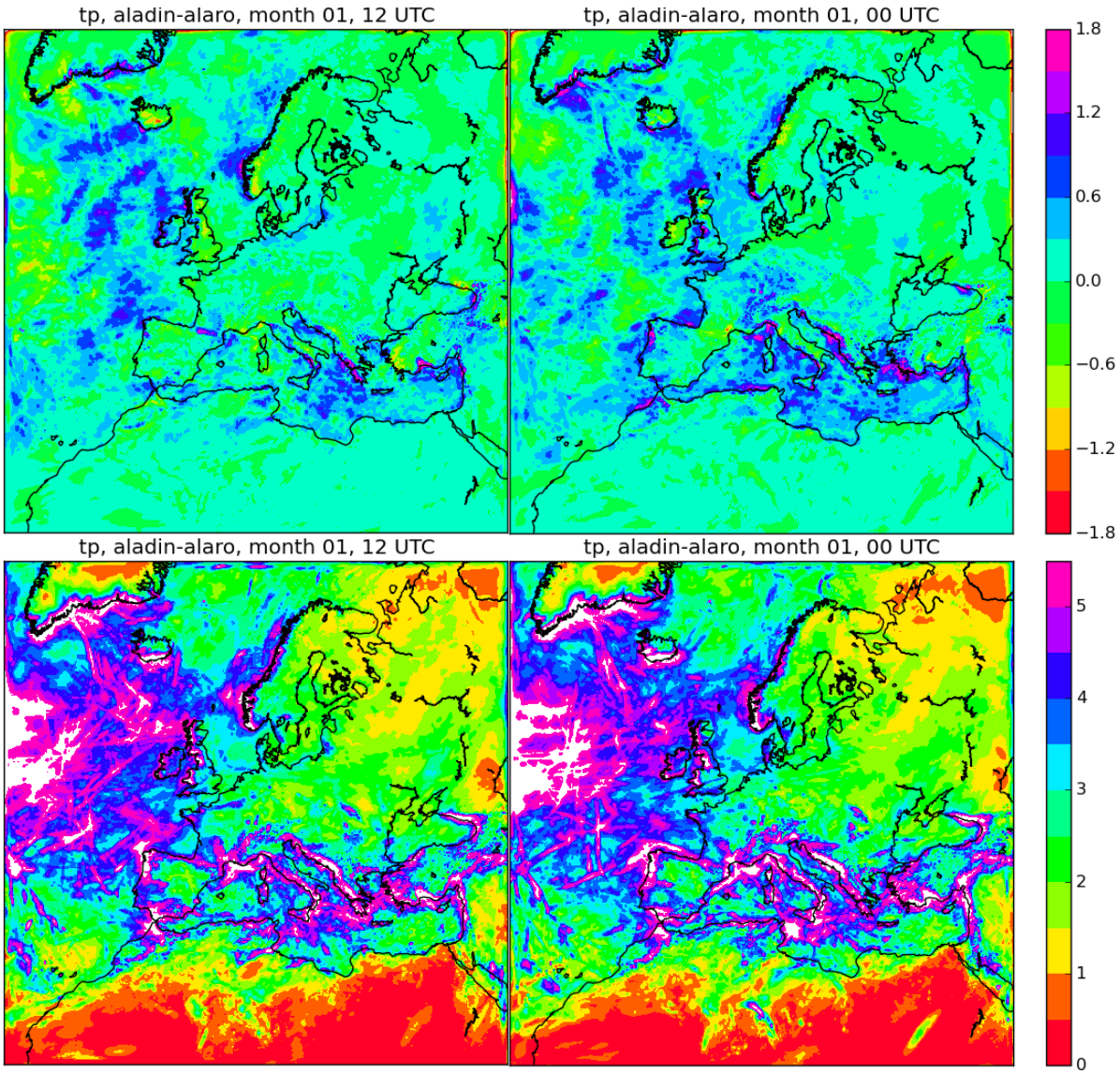

Figure 14. Mean (upper row) and standard deviation (lower row) of total precipitation difference between ALADIN-RA and ALARO-Ra in January. Left and right panels depict the values for 0 and 12 UTC, respectively. Total precipitation in units of mm/12hours is calculated as differences between the accumulated 24-hour and 12-hour forecasts. The colour intervals are in steps of 0.3 mm/12hours for the mean, and in steps of 0.5 mm/12hours for the standard deviation. White areas mark values beyond the given limits.

Figure displays the statistics for the precipitation difference in January for 0 and 12 UTC. The mean differences in the upper row illustrate the fact that ALADIN-RA has generally more precipitation than ALARO-RA. It should be noted that in large parts of the land area the mean difference lies between -0.3 and 0.3 mm per 12 hours. The standard deviation of the precipitation difference shows largest values of slightly larger than 5.5 mm per 12 hours over the North Atlantic, Atlantic and Mediterranean coasts. For continental Europe, the standard deviation amounts mostly to values less than 3 mm per 12 hours. Taken into account the general noisiness of the fields, a clear diurnal cycle for January data cannot be stated for neither mean nor standard deviation.

For July, the mean temperature differences are shown in Figure for the different analysis hours during the day. While the difference remains mainly below 1 K, a clear diurnal cycle is visible in Northern Africa. During 12 and 18 UTC, ALADIN-RA has higher mean temperatures in the western part of North Africa with values up to 5 K, while ALARO-RA is warmer in the eastern part especially at 12 UTC. During 0 and 6 UTC, the difference has an almost opposite pattern, with ALARO-RA being warmer in the western part.

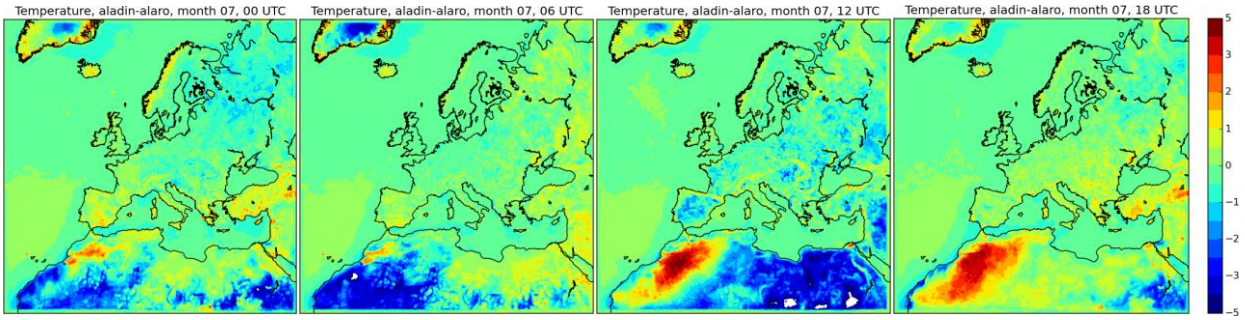

Figure 15. Mean temperature difference between ALADIN-RA and ALARO-RA for July. The panels show the values for 0, 6, 12, and 18 UTC from left to right. The colour intervals are in steps of 0.5 between -3 and +3 K, and in steps of 1 K between absolute values of 3 and 5. White areas mark values beyond the given limits.

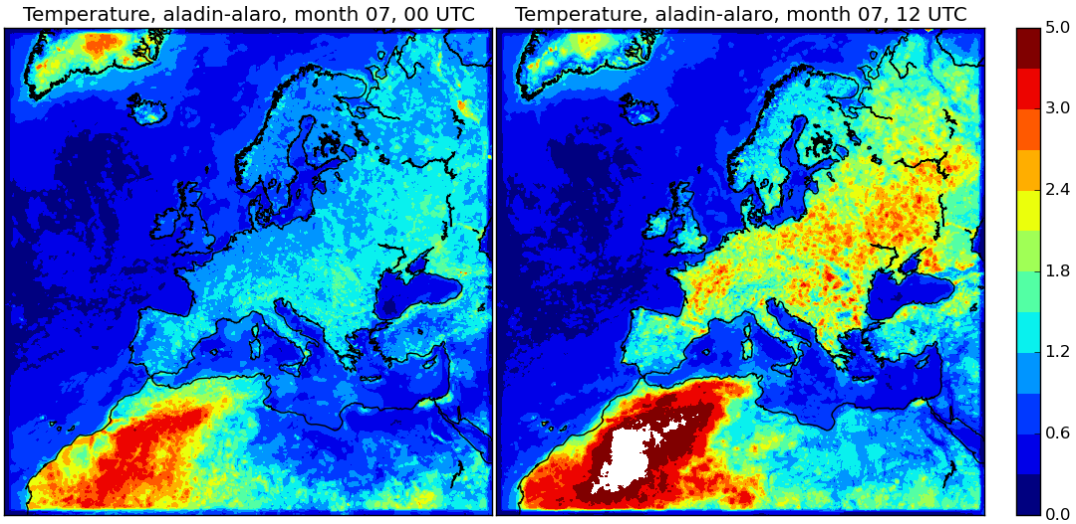

Figure 1611. Daily standard deviation of temperature difference between ALADIN-RA and ALARO-RA in July. Panels depict the values for 0 (left) and 12 UTC (right). The colour intervals are in steps of 0.3 up to 3 K, and in steps of 1 K up to 5. White areas mark values beyond the given limits.

The daily standard deviation of the temperature difference for July shows a clear diurnal cycle (Figure 1611). In the western part of Northern Africa, the standard deviation reaches largest values slightly larger than 5 K around 12 UTC. Over most parts of Europe, the reanalysis uncertainty in July is minimal around 0 UTC with values smaller than 1.5 K. At 12 UTC, the precision decreases to values between 2 and 3 K, locally up to 4 K (right panel in Figure 1611).

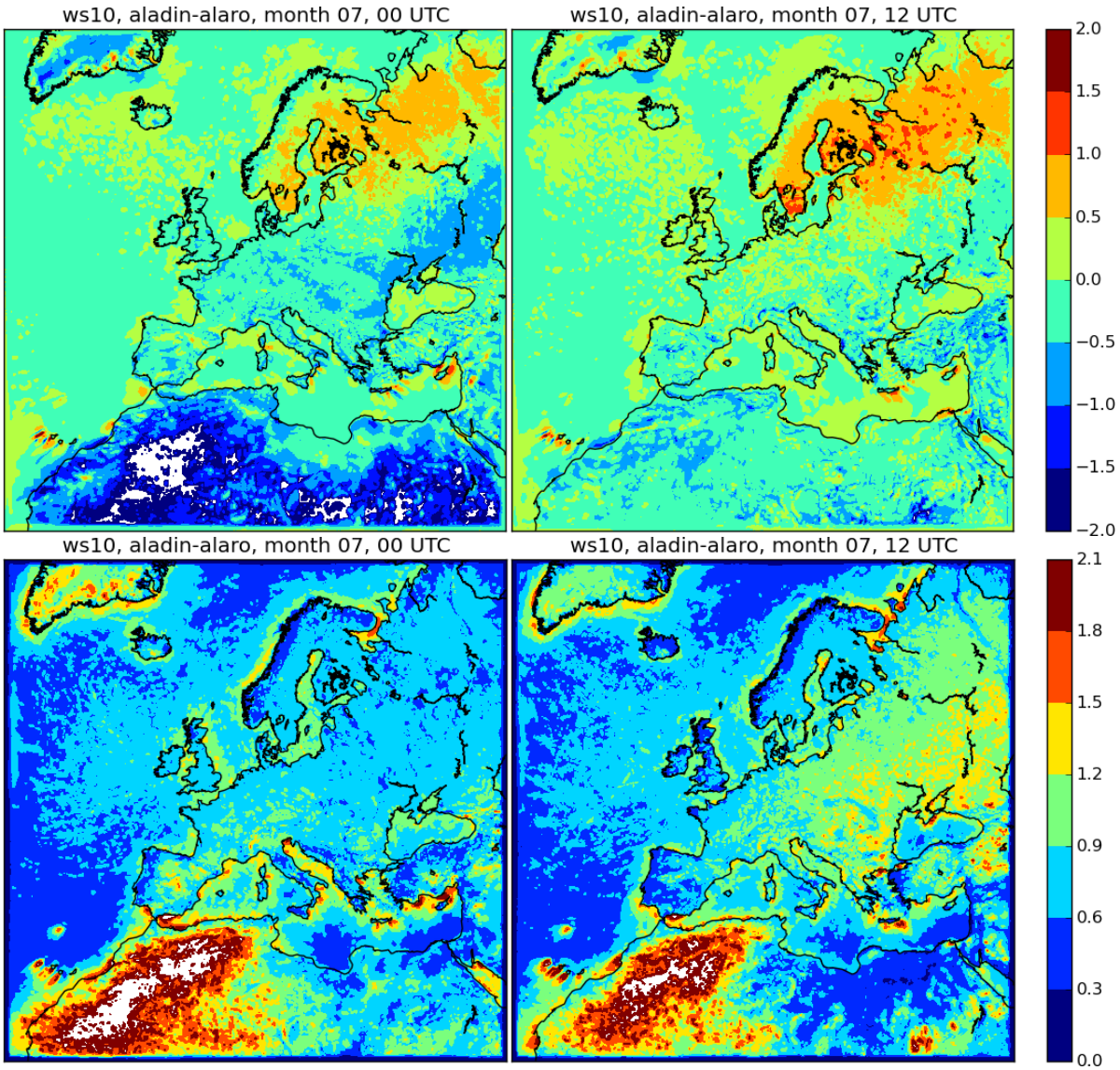

Figure 17. Mean (upper row) and daily standard deviation (lower row) of 10m-wind speed difference between ALADIN- and ALARO-RA for July. Left and right panels depict the values for 0 and 12 UTC, respectively. The colour intervals are in steps of 0.5 m/s for the mean and in steps of 0.3 m/s for the standard deviation.

For the mean 10m-wind speed difference between ALADIN-RA and ALARO (Figure), the above findings from the 5-year climatology are confirmed. ALADIN-RA contains stronger winds than ALARO-RA in the north-eastern part of the domain with largest values of 1.5 m/s at 12 UTC. In North Africa, a clear diurnal

cycle is visible in the wind speed difference, where ALARO-RA has stronger winds than ALADIN-RA with largest absolute wind difference of slightly more than 2 m/s at 0 UTC.

The daily standard deviation of the 10m-wind speed is below 0.9 m/s for most parts of Europe at 0 UTC. During the day, values are higher, but mostly below 1.5 m/s in Europe. Similar to the daily standard deviation of temperature (Figure 1611), largest values for the standard deviation of the wind are found in the western part of Northern Africa. However, the daily cycle for the wind speed displays slightly larger values during 0 UTC than during 12 UTC. During both times, values can be slightly higher than 2.1 m/s.

Mean and daily standard deviation of the total precipitation differences between ALADIN-RA and ALARO-RA are displayed in Figure. The left column shows the values for the first half of the day (0-12 UTC), the right column for the second (12-0 UTC). As can be seen in the mean differences (upper row), ALADIN-RA has generally a wetter July with largest differences at 0 UTC, especially in mountainous terrain with values up to 1.8 mm per 12 hours. An interesting feature occurs at the north-western border of the domain with a different behavior of the data sets at the boundary.

The daily standard deviation of the total precipitation difference varies in most parts of Europe between 1 and 3.5 mm per 12 hours. Locally, especially in connection with high topography, values up to 5 mm per 12 hours can be reached. The daily cycle shows maximum uncertainty for the July precipitation during the second half of the day.

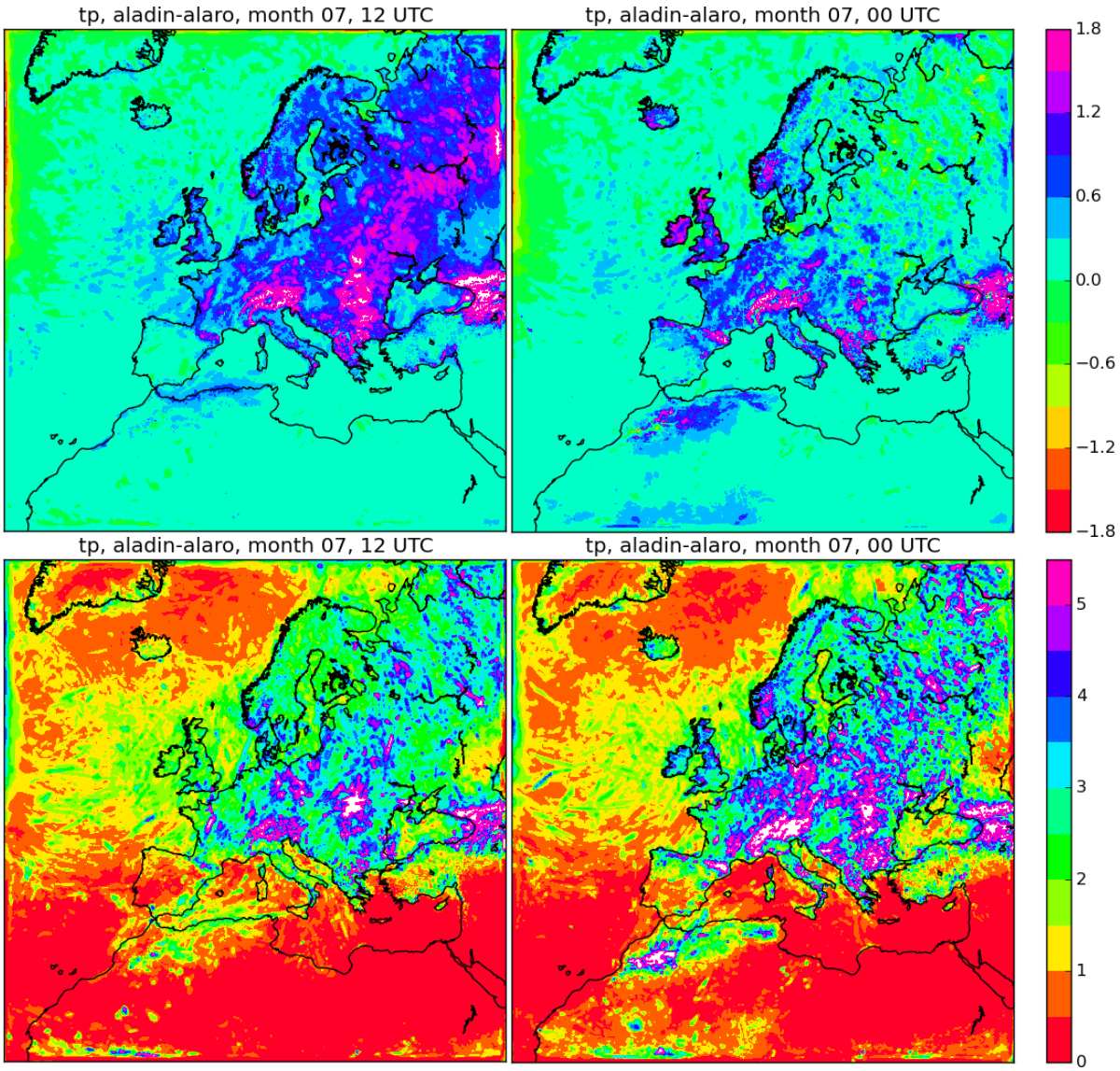

Figure 18. Mean (upper row) and standard deviation (lower row) of total precipitation difference between ALADIN-RA and ALARO-Ra in July. Left and right panels depict the values for 0 and 12 UTC, respectively. Total precipitation in units of mm/12hours is calculated as differences between the accumulated 24-hour and 12-hour forecasts. The colour intervals are in steps of 0.3 mm/12hours for the mean, and in steps of 0.5 mm/12hours for the standard deviation. White areas mark values beyond the given limits.

Verification

The HARMONIE verification system WebgraF has been used to verify the two model forecasts for the 5-year period. Due to the amount of data, the number of parameters that were verified had to be reduced. For the surface, wind speed at 10 meters altitude, temperature and dew point at 2 meters, mean sea level pressure, cloud cover and 12 hour accumulated precipitation have been verified. For upper air: temperature, wind speed and relative humidity. The data is seasonally divided. The forecasts are verified against the same observations that were used for the initial analysis. Below some examples are shown and commented.

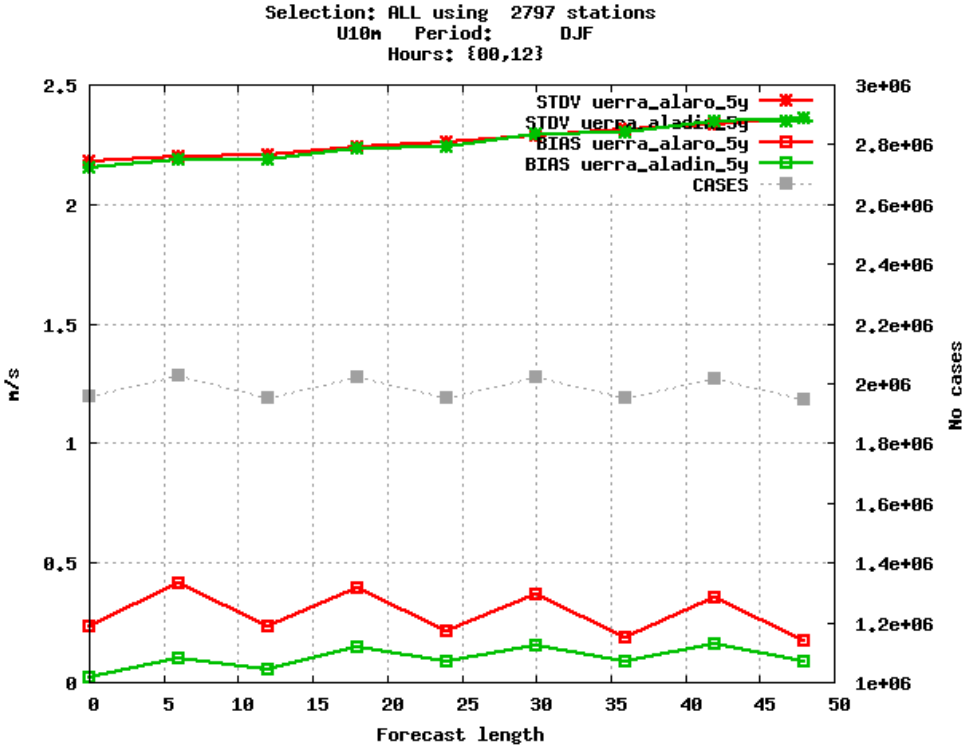

Figure 19. Standard deviation and bias for 10 meter wind speed winter (DJF), ALADIN (green), ALARO (red).

For 10-m wind speed in winter a slightly better STDV and a smaller bias for ALADIN is shown.

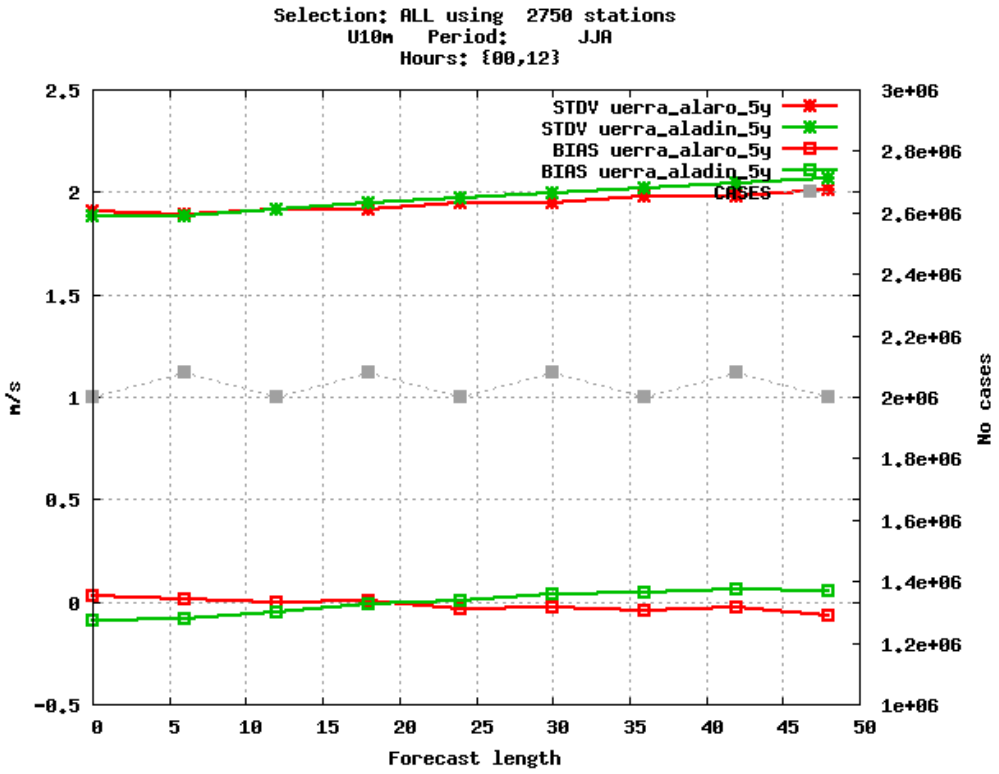

Figure 20. Standard deviation and bias for 10 meter wind speed winter (JJA), ALADIN (green), ALARO (red).

For the summer 10 meter wind speed there is a slightly better STDV for ALARO. The bias is small for both models.

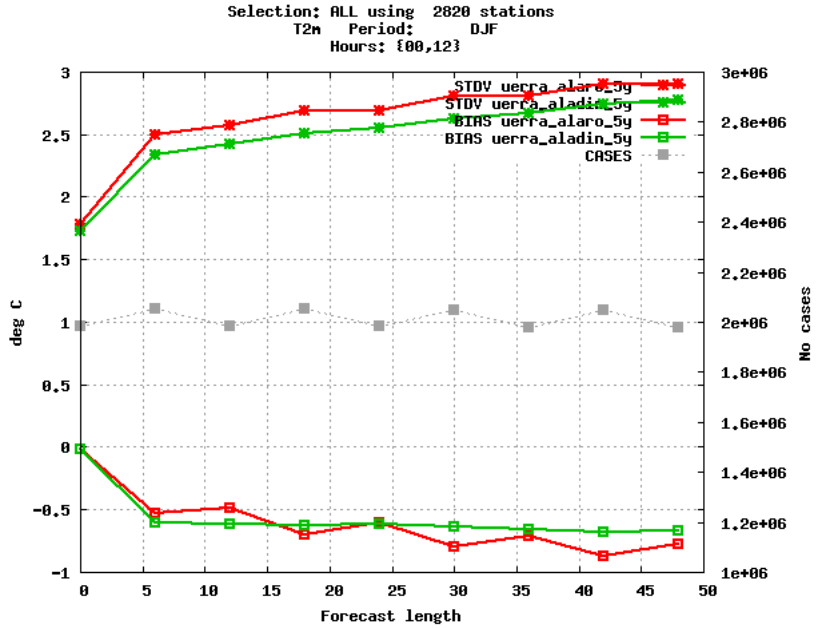

Figure 21. Standard deviation and bias for 2 meter temperature winter (DJF), ALADIN (green), ALARO (red).

A clear advantage for ALADIN regarding STDV for 2 meter winter temperatures can be seen. Both models have a negative bias, slightly worse for ALARO.

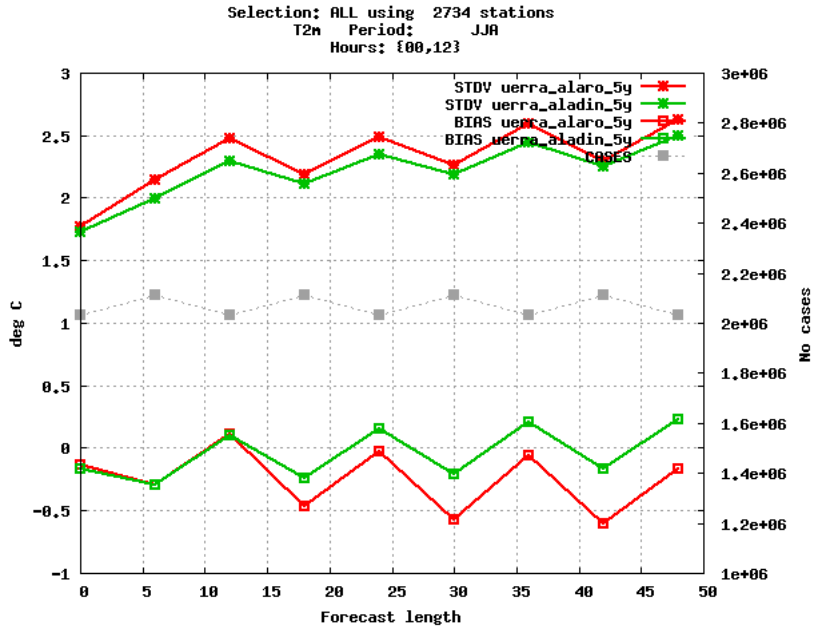

Figure 22. Standard deviation and bias for 2 meter temperature summer (JJA), ALADIN (green), ALARO (red).

For summer 2 meter temperatures ALADIN has the lowest STDV and a bias that is closer to zero than ALARO.

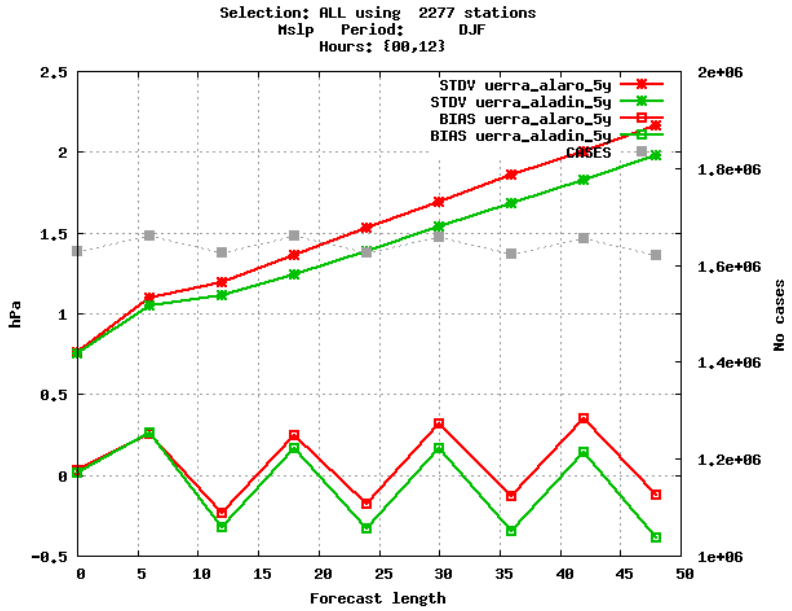

Figure 23. Standard deviation and bias for mean sea level pressure winter (DJF), ALADIN (green), ALARO (red).

Slightly lower STDV in ALADIN for mean sea level pressure can be found. Both models show a bias.

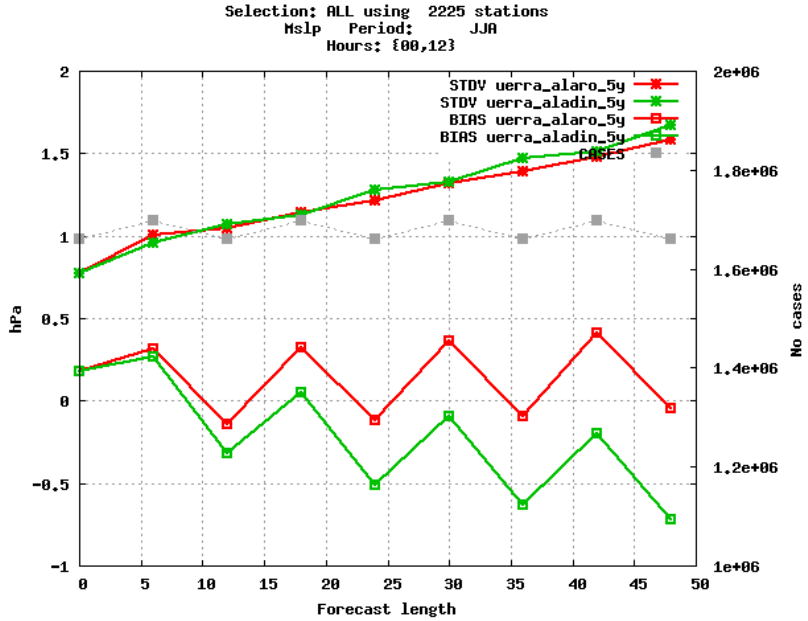

Figure 24. Standard deviation and bias for mean sea level pressure summer (JJA), ALADIN (green), ALARO (red).

A small advantage for ALARO can be seen in STDV mean sea level pressure in summer. There is strange negative trend in the bias for ALADIN.

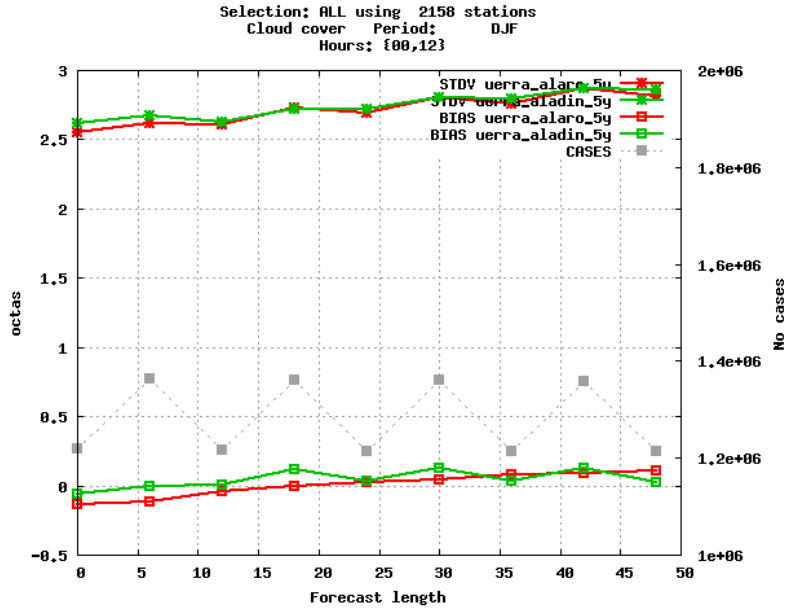

Figure 25. Standard deviation and bias for total cloud cover winter (DJF), ALADIN (green), ALARO (red).

Both models show very similar results for total cloud cover winter. Bias is very close to zero.

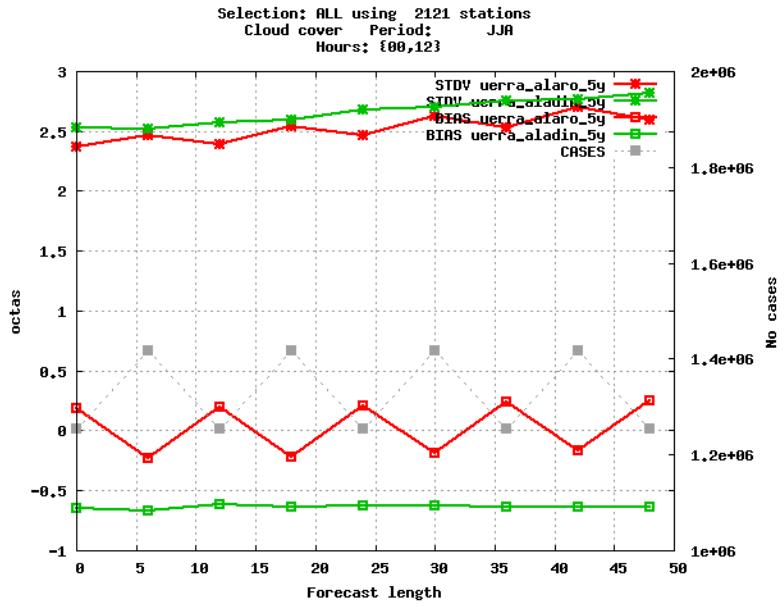

Figure 26. Standard deviation and bias for total cloud cover summer (JJA), ALADIN (green), ALARO (red).

For summer total cloud cover the ALARO model shows a little better result than ALADIN.

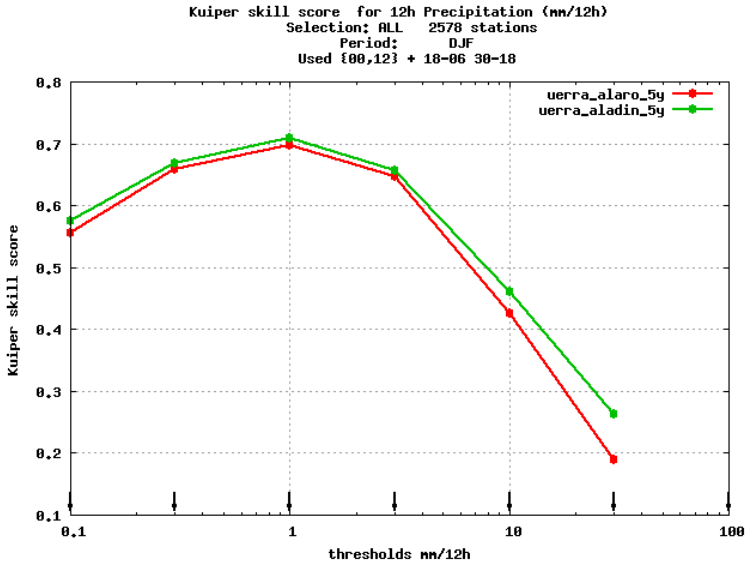

Figure 27. Kuiper skill score for winter 12 hours accumulated precipitation at different thresholds. ALADIN (green), ALARO (red).

A small advantage for ALADIN can be seen for all precipitation classes during winter.

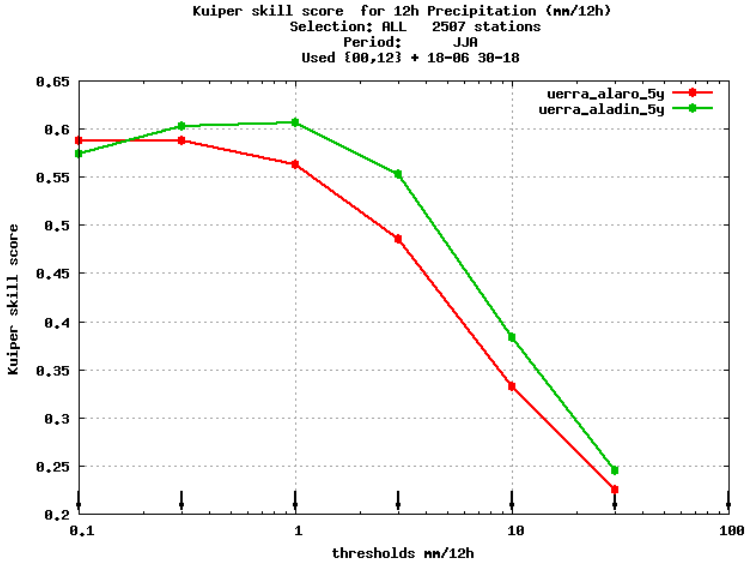

Figure 28. Kuiper skill score for summer 12 hours accumulated precipitation at different thresholds. ALADIN (green), ALARO (red).

For summer precipitation the ALADIN advantage is bigger for most classes, while ALARO is slightly better for the smallest amounts.

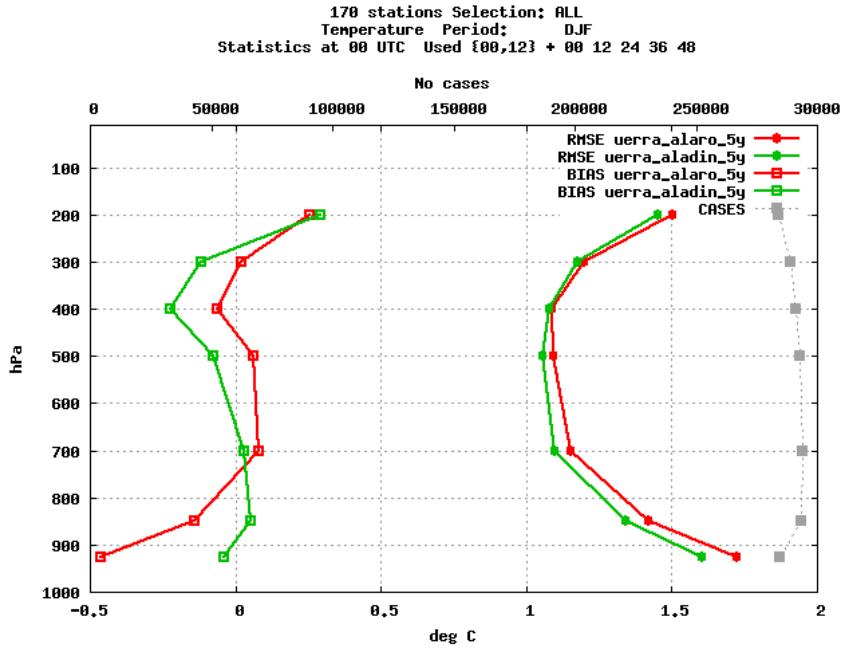

Figure 29. RMSE and bias for temperature profiles winter (DJF), 00 UTC-runs. ALADIN (green), ALARO (red).

ALADIN has slightly lower RMSE-values throughout the whole profile. The ALADIN bias is close to zero in the lower parts, while the ALARO bias is a little better in the upper levels.

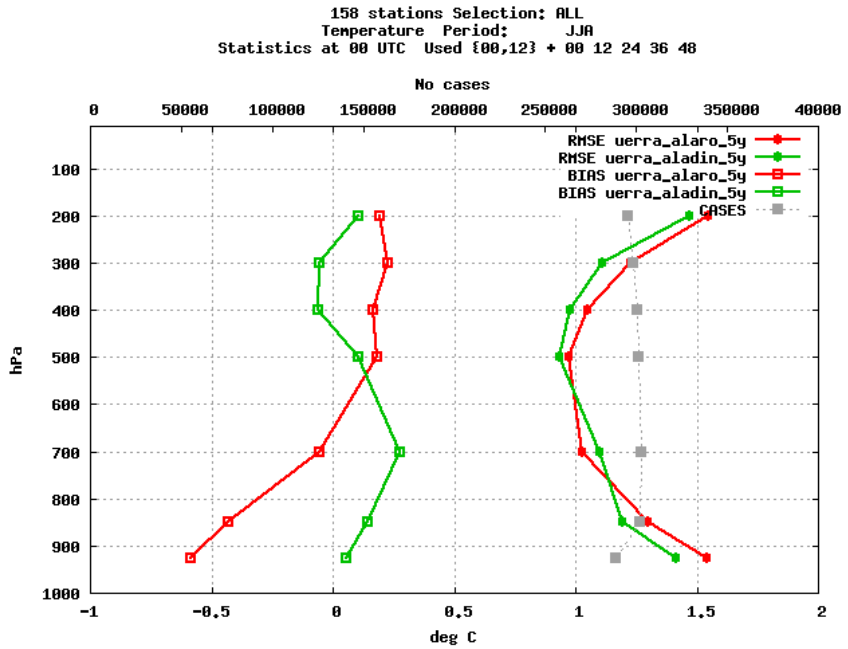

Figure 30. RMSE and bias for temperature profiles summer (JJA), 00 UTC-runs. ALADIN (green), ALARO (red).

Again ALADIN has the lowest RMSE for almost all levels.

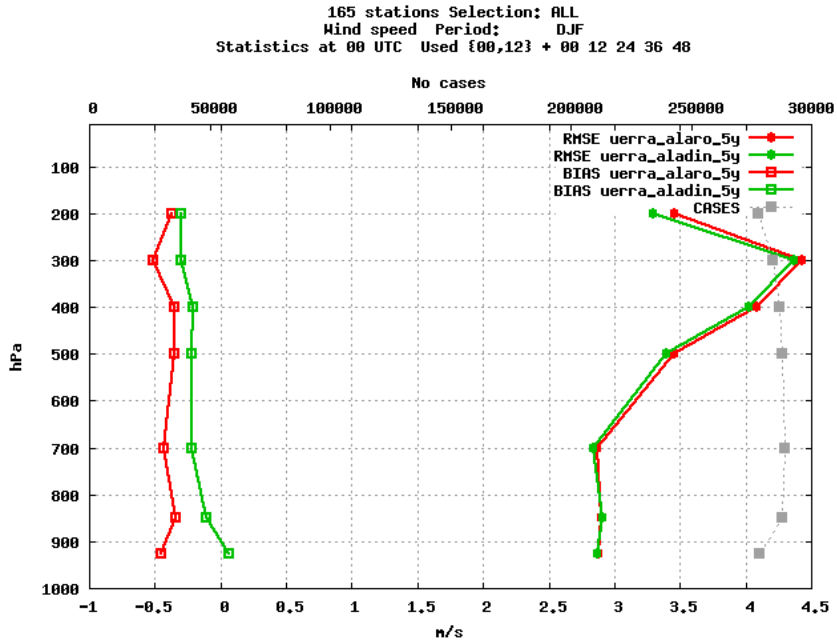

Figure 31. RMSE and bias for wind speed profiles winter (DJF), 00 UTC-runs. ALADIN (green), ALARO (red).

Almost identical RMSE values for both models with a very small advantage for ALADIN. The bias is also a little closer to zero for ALADIN.

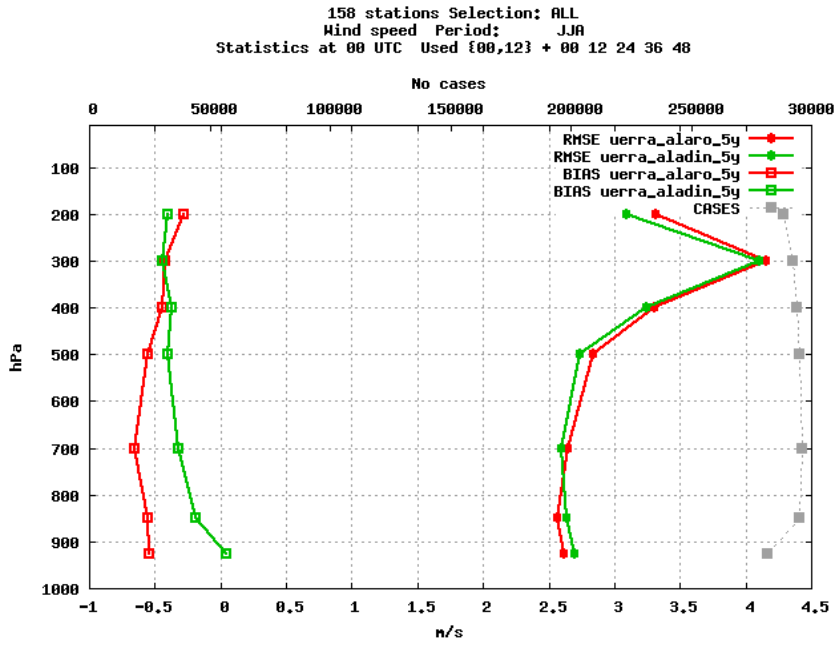

Figure 32: RMSE and bias for wind speed profiles summer (JJA), 00 UTC-runs. ALADIN (green), ALARO (red).

Lower RMSE-values are seen for ALADIN on the majority of the levels, also smaller bias for most parts.

The verification shows that for most variables there is an advantage for ALADIN. ALARO is a little bit better for 10-m wind speed in the summer and also for total cloud cover both summer and winter. For the rest of the figures shown the scores are either very close or there is an ALADIN advantage.

5. Conclusions and final decision

The goals of this study were:

1) To setup the HARMONIE system for regional reanalysis over Europe
2) To generate a mini-ensemble reanalysis data set over 5 years in order to estimate uncertainties in the reanalysis products
3) To compare two different physics packages in the verification of the reanalyses and to select the one that is performing better for the long reanalysis production

The HARMONIE system was set up over Europe and two reanalysis data sets were produced for the years 2006 to 2010. Two different physics packages, ALADIN and ALARO were used producing two 5-year UERRA reanalysis data sets. For the inclusion of the large-scale information from the global reanalysis, the approach of an additional term in the cost function is employed. Unfortunately (or fortunately) it was discovered that the implementation of this Jk-formulation is not correct. As a result the minimisation does not converge properly.

The monitoring of the observation usage shows however that the data assimilation schemes works to a large degree. The comparison of the first guess and the analysis with the observations confirms that the

assimilation works properly in observation dense areas. The problems arise in areas with few observations where the information from the larger scale global model is given more influence.

The mini-ensemble of UERRA-reanalyses with HARMONIE allowed us to examine the uncertainties in the reanalysis products. The monthly mean and daily standard deviation of the differences between ALADIN- and ALARO-RA was determined for different variables, for January and July and for different hours of the day. The mean difference will provide an estimate for the systematic error or accuracy in the reanalysis, while the standard deviation of the reanalysis difference yields a measure for the unbiased uncertainty or precision of the reanalysis.

For the largest part of the domain, the mean differences for the 2m-temperature amount to values less than 1 K, for the 10m-wind speed less than 1 m/s, and for the total precipitation less than 0.3 (1.2) mm/12 hours in January (July). Locally, especially in connection with coast lines and topography, higher values can occur. As for the standard deviation of the differences, the largest part has uncertainties less than 1.5 K for 2m-temperature, less than 1.2 m/s for 10m-wind speed and less than 3.5 mm/12 hours for total precipitation. Here, local variations can also be considerably higher. Furthermore, a clear diurnal cycle was apparent for certain variables in certain seasons, especially for the standard deviation of the 2m-temperature in January and July and for the total precipitation in July. Larger differences in 2m-temperature and 10m-wind speed were found in the western part of Northern Africa. These larger differences in Africa and areas with mountainous terrain can be an effect of the error in the Jk-implementation. It is in these areas with few observations and steep orography that the effect of Jk will be the largest. This issue requires a deeper going examination.

The verification of the two UERRA-reanalyses was conducted for numerous near-surface variables as well as for profiles in temperature and wind. For most seasons and most variables, the ALADIN reanalysis performed better than the ALARO reanalysis. Due to this better performance it is decided that ALADIN is selected as the physics package to be used in the long reanalysis production from 1960 to 2010.

Due to the problems found in the minimisation the period needs to be re-run when the problem is located and solved. Comparisons will be made to the results presented here but it is believed that this will not change the conclusions from the verification. The reason for this is that in areas with good observation coverage the Jo-term dominates the cost function and the verifications are made against observations. In order to produce a good data set in the entire model domain however, the 5 year period needs to be re-run. For ALADIN this will be done anyway as part of the long re-analysis.

References

ALADIN International Team, 1997: The ALADIN project: Mesoscale modelling seen as a basic tool for weather forecasting and atmospheric research. WMO Bull., 46, 317–324.

Bechtold, P., Bazile, E., Guichard, F., Mascart, P., and Richard, E.: A mass flux convection scheme for regional and global models, Q. J. Roy. Meteor. Soc., **127**, 869–886, 2001.

Belamari, S., and A. Pirani, 2007: Validation of the optimal heat and momentum fluxes using the ORCA2-LIM global ocean-ice model. Marine environment and security for the European area. Integrated Project (MERSEA IP), Deliverable D4.1.3, 88 pp.Berre, L.: Estimation of synoptic and mesoscale forecast error covariances in a limited-area model. *Mon. Wea. Rev.*, **128**, 644–667, 2000.

Bougeault, P.: A simple parameterization of the large-scale effects of cumulus convection, Mon. Weather Rev., **113**, 2108–2121, 1985.

Bougeault, P. and Lacarrère, P.: Parameterization of orography-induced turbulence in a mesobeta-scale model, Mon. Weather Rev., **117**, 1872–1890, 1989.

Bouteloup, Y., Bouyssel, F., and Marquet, P.: Improvments of Lopez's prognostic large scale cloud and precipitation scheme, ALADIN Newslett., **28**, 66–73, 2005.

Brousseau, P., and coauthors: A prototype convective-scale data assimilation system for operation: The AROME-RUC. *HIRLAM Tech. Rep*., **68**, 23–30, 2008.

Brousseau, P., L. Berre, F. Bouttier, and G. Desroziers: Flow-dependent background-error covariances for a convective-scale data assimilation system. *Q. J. R. Meteorol. Soc.*, **138**, 310–322, 2012.

Bubnova, R., Hello, G., Bnard, P. and Geleyn, J.-F. 1995. Integration of the fully-elastic equations cast in the hydrostatic pressure terrain-following coordinate in the framework of the ARPEGE/ALADIN NWP system. Mon. Weather Rev. 123, 515–535.

Catry, B., Geleyn, J. F., Bouyssel, F., Cedilnik, J., Brozkova, R., Derkova, M., and Mladek, R.: A new sub-grid scale lift formulation in a mountain drag parametarisation scheme, Meteorol.Z., **17**, 193–208, 2008.

Charnock, H., 1955: Wind stress over a water surface. Quart. J. Roy. Meteor. Soc., **81**, 639–640.

Cuxart, J., Bougeault, P., and Redelsperger, J. L.: A turbulence scheme allowing for mesoscale and large-eddy simulations, Q. J. Roy. Meteor. Soc., **126**, 1–30, 2000.

Dahlgren P.: Using Jk in AROME 3DVAR: Some initial tests HIRLAM Newsletter No. 59 Dec 2012, p3-9, 2012.

Fouquart, Y. and Bonnel, B.: Computations of solar heating of the earth's atmosphere: a new parameterization, Beitr. Phys. Atmosph., **53**, 35–62, 1980.

Geleyn, J.-F., B. Catry, Y. Bouteloup, and R. Brožková, 2008: A statistical approach for sedimentation inside a microphysical precipitation scheme. Tellus, 60A, 649–662, doi:10.1111/j.1600-0870.2008.00323.x.

Gerard, L., J.-M. Piriou, R. Brožková, J.-F. Geleyn, and D. Banciu, 2009: Cloud and precipitation parameterization in a meso-gamma-scale operational weather prediction model. Mon. Wea. Rev., 137, 3960–3977.

Guidard V. and Fischer C.: Introducing the coupling information in a limited-area variational assimilation, *Q. J. R. Meteorol. Soc.*, **134**, 723-736, 2008.

Gustafsson, N., Berre, L., Hörnquist, S., Huang, X.-Y., Lindskog, M., Navascués, B., Mogensen, K.S., Thorsteinsson, S.: Three-dimensional variational data assimilation for a limited area model. Part I: general formulation and the background error constraint. *Tellus*, **53A**, 425–446, 2001.

Lindskog, M., Gustafsson, N., Navascués, B., Mogensen, K.S., Huang, X.-Y., Yang, X., Andræ, U., Berre, L., Thorsteinsson, S., Rantakokko, J.:. Three-dimensional variational data assimilation for a limited area model. Part II: observation handling and assimilation experiments. *Tellus*, **53A**, 447–468, 2001.

Liu, W. T., K. B. Katsaros, and A. Businger, 1979: Bulk parameterization of air–sea exchanges of heat and water vapor including the molecular constraints at the interface. J. Atmos. Sci., **36**, 1722–1735.

Lopez, P.: Implementation and validation of a new prognostic large-scale cloud and precipitation scheme for climate and data-assimilation purposes, Q. J. Roy. Meteor. Soc., **128**, 229–257, 2002.

Masson V (2000) A physically-based scheme for the urban energy budget in atmospheric models. Boundary-Layer Meteorol, **94** ,357–397

Masson, V., J.-L. Champeaux, F. Chauvin, C. Meriguet, and R. Lacaze, 2003: A global database of land surface parameters at 1-km resolution in meteorological and climate models. J. Climate, **16**, 1261–1282.

Mlawer, E. J., Taubman, S. J., Brown, P. D., Iacono, M. J., and Clough, S. A.: RRTM, a validated correlated-k model for the longwave, J. Geophys. Res., **102**, 16663–16682, 1997.

Morcrette, J. J.: Radiation and cloud radiative properties in the ECMWF operational weather forecast model, J. Geophys. Res. D, **96**, 9121–9132, 1991.

Montmerle, T., and L. Berre: Diagnosis and formulation of heterogeneous background-error covariances at the mesoscale. *Q. J. R. Meteorol. Soc.*, **136**, 1408–1420, 2010.

Noilhan J. and S. Planton: A Simple Parameterization of Land Surface Processes for Meteorological Models. *Mon. Wea. Rev.*, **117**, 536–549, 1989.

Ritter, B., and J.-F. Geleyn, 1992: A comprehensive radiation scheme for numerical weather prediction models with potential applications in climate simulations. Mon. Wea. Rev., 120, 303–325.

Taillefer, F.: CANARI - Technical Documentation - Based on ARPEGE cycle CY25T1 (AL25T1 for ALADIN), available at htp://www.cnrm.meteo.fr/aladin/, 2002.

Seity Y., P. Brousseau, S.Malardel, G. Hello, P. Bénard, F. Bouttier, C. Lac and V. Masson: The AROME-France Convective-Scale Operational Model, *Monthly Weather Review*, **139**, 976-991, 2011.

Smith, R. N. B.: A scheme for predicting layer clouds and their water content in a general circulation model, Q. J. Roy. Meteor. Soc., **116**, 435–460, 1990.

Váňa, F., P. Bénard, J.-F. Geleyn, A. Simon, and Y. Seity, 2008: Semi-Lagrangian advection scheme with controlled damping: An alternative to nonlinear horizontal diffusion in a numerical weather prediction model. Quart. J. Roy. Meteor. Soc., 134, 523–537, doi:10.1002/qj.220.